2004-06

Grain size control in AA5083: thermomechanical processing and particle stimulated nucelation

Deffenbaugh, Kristen Lynn

Monterey, California. Naval Postgraduate School

http://hdl.handle.net/10945/1162

NAVAL
POSTGRADUATE
SCHOOL

MONTEREY, CALIFORNIA

THESIS

**GRAIN SIZE CONTROL IN AA5083:
THERMOMECHANICAL PROCESSING AND PARTICLE
STIMULATED NUCELATION**

by

Kristen Lynn Deffenbaugh

June 2004

Thesis Advisor: Terry R. McNelley

THIS PAGE INTENTIONALLY LEFT BLANK

REPORT DOCUMENTATION PAGE		*Form Approved OMB No. 0704-0188*

Public reporting burden for this collection of information is estimated to average 1 hour per response, including the time for reviewing instruction, searching existing data sources, gathering and maintaining the data needed, and completing and reviewing the collection of information. Send comments regarding this burden estimate or any other aspect of this collection of information, including suggestions for reducing this burden, to Washington headquarters Services, Directorate for Information Operations and Reports, 1215 Jefferson Davis Highway, Suite 1204, Arlington, VA 22202-4302, and to the Office of Management and Budget, Paperwork Reduction Project (0704-0188) Washington DC 20503.

1. AGENCY USE ONLY *(Leave blank)*	2. REPORT DATE June 2004	3. REPORT TYPE AND DATES COVERED Master's Thesis	
4. TITLE AND SUBTITLE: Title (Mix case letters) Grain Size Control in AA5083: Thermomechanical Processing and Particle Stimulated Nucleation		5. FUNDING NUMBERS	
6. AUTHOR(S) Kristen Lynn Deffenbaugh			
7. PERFORMING ORGANIZATION NAME(S) AND ADDRESS(ES) Naval Postgraduate School Monterey, CA 93943-5000		8. PERFORMING ORGANIZATION REPORT NUMBER	
9. SPONSORING /MONITORING AGENCY NAME(S) AND ADDRESS(ES) N/A		10. SPONSORING/MONITORING AGENCY REPORT NUMBER	

11. SUPPLEMENTARY NOTES   The views expressed in this thesis are those of the author and do not reflect the official policy or position of the Department of Defense or the U.S. Government.

12a. DISTRIBUTION / AVAILABILITY STATEMENT Approved for public release; distribution is unlimited	12b. DISTRIBUTION CODE A

13. ABSTRACT (maximum 200 words)

Superplastic forming is an emerging industrial technology that allows the production of complex shapes in metallic materials including aluminum. A critical characteristic of materials that are capable of sustaining superplastic forming is a fine grain size. In this study a commercial aluminum-magnesium-manganese alloy received in the as-cast condition was subjected to various thermomechanical processes intended to refine the grain size. Particle stimulated nucleation (PSN) theory was employed to develop the thermomechanical processes. These processes all involved initial homogenization and hot working. Subsequent annealing treatments were intended to control the size and size distribution of second phase particles, such as Al_6Mn. Strain energy was introduced through cold rolling followed by recrystallization anneals. Samples were analyzed using orientation-imaging microscopy to examine the effect of processing variables on the recrystallized grain size.

14. SUBJECT TERMS superplasticity, grain size control, particle stimulated nucleation, PSN, thermomechanical processing, AA5083, aluminum-magnesium-manganese			15. NUMBER OF PAGES 65
			16. PRICE CODE
17. SECURITY CLASSIFICATION OF REPORT Unclassified	18. SECURITY CLASSIFICATION OF THIS PAGE Unclassified	19. SECURITY CLASSIFICATION OF ABSTRACT Unclassified	20. LIMITATION OF ABSTRACT UL

NSN 7540-01-280-5500

Standard Form 298 (Rev. 2-89)
Prescribed by ANSI Std. 239-18

i

THIS PAGE INTENTIONALLY LEFT BLANK

GRAIN SIZE CONTROL IN AA5083: THERMOMECHANICAL PROCESSING AND PARTICLE STIMULATED NUCLEATION

Kristen L. Deffenbaugh
Ensign, United States Navy
B.S., United States Naval Academy, 2003

Submitted in partial fulfillment of the
requirements for the degree of

MASTER OF SCIENCE IN MECHANICAL ENGINEERING

from the

**NAVAL POSTGRADUATE SCHOOL
June 2004**

Author: Kristen Lynn Deffenbaugh

Approved by: Terry R. McNelley
                 Thesis Advisor

                 Anthony J. Healey
                 Chairman, Department of Mechanical and Astronautical
                 Engineering

THIS PAGE INTENTIONALLY LEFT BLANK

ABSTRACT

Superplastic forming is an emerging industrial technology that allows the production of complex shapes in metallic materials including aluminum. A critical characteristic of materials that are capable of sustaining superplastic forming is a fine grain size. In this study a commercial aluminum-magnesium-manganese alloy received in the as-cast condition was subjected to various thermomechanical processes intended to refine the grain size. Particle stimulated nucleation (PSN) theory was employed to develop the thermomechanical processes. These processes all involved initial homogenization and hot working. Subsequent annealing treatments were intended to control the size and size distribution of second phase particles, such as Al_6Mn. Strain energy was introduced through cold rolling followed by recrystallization anneals. Samples were analyzed using orientation-imaging microscopy to examine the effect of processing variables on the recrystallized grain size.

THIS PAGE INTENTIONALLY LEFT BLANK

TABLE OF CONTENTS

LIST OF FIGURES

LIST OF TABLES

THIS PAGE INTENTIONALLY LEFT BLANK

ACKNOWLEDGMENTS

THIS PAGE INTENTIONALLY LEFT BLANK

I.   INTRODUCTION

A.   SUPERPLASTICITY

Superplasticity is the ability of a material to undergo extensive tensile elongations.   Though superplasticity may have been taken advantage of as early as ancient times with the hand-forming of detailed shapes, it was not until 1912 that superplasticity was identified as a distinct phenomenon.   It remained primarily of research interest until 1962 when Backofen and his colleagues published a paper demonstrating the formability of an aluminum-zinc alloy into a practical shape. Research in the field expanded dramatically as the process proved its potential for industrial application. [1,2]

The aerospace industry first began widespread implementation of superplastic forming (SPF) of parts, as there has always been a need to use high strength-to-weight materials such as aluminum and titanium.   The forming of complex, one-piece components replaced the need for welding and fastening of several pieces there by saving both weight and production time. Superplastically formed parts are also free of residual stresses, in addition to having a good surface finish and no spring back. Examples of superplastically formed aircraft pieces are landing gear doors, wing tips, engine nacelles, and stiffening panels. [1-3]

Over time, applications have expanded to include both architecture and rail components. Used primarily as decoration, architectural pieces take advantage of the intricate details attainable with SPF. In the rail industry, superplastic aluminum panels have proven to be beneficial for both interior and exterior use.   In addition to the traditional benefits, using these parts as interior body panels improves safety, eliminating the potential for toxic fumes upon burning of conventional plastic or polymer parts. An example of an internal panel is seen in Figure 1. [3]

Figure 1.   Example of superplastically formed panels for rail use [3]

In the automotive industry, manufacturers are considering SPF for several reasons. Recently, as fuel prices rise steadily, there is a renewed interest in improving fuel efficiency. The replacement of steel with lightweight materials of sufficient strength would improve fuel efficiency. In addition, SPF, if practical, could provide manufacturers with numerous options in designing car bodies due to reduced hardware costs and ability to form complex geometries. [3,4]

B.   LIMITATIONS OF SUPERPLASTICITY

Traditional forming of sheet steel for automotive applications is through stamping followed by assembly by welding. [5] Potential candidate aluminum alloys that are strong enough for automotive applications do not have sufficient ductility to be formed in such a manner. However, some of these alloys can be formed superplastically.

Despite the promises of superplastic forming, the technology is limited in its commercial application primarily because of long forming times. In many applications, it is not unusual to have local elongations in excess of 200%. [1,3] At current forming (strain) rates of approximately 10^{-4} to 10^{-3} per second, manufacture of one part can take on the order of an hour. Compared to the current methods which take only seconds to produce parts, this severely limits production and renders the process less cost effective. In addition, non-uniform thinning and cavitation can occur leading to local weakness and failure in superplastically formed materials. [4] Current research addresses these issues in the hopes of making superplastic forming a more practical process to implement.

2

II. BACKGROUND

A. SUPERPLASTIC FORMING

1. The Forming Process

Though it is not uncommon for superplastic alloys to exhibit elongations between 500% and 1000%, typical forming only requires elongation of 200% to 300% for even very complex parts. [1] The large tensile deformations that occur during superplastic forming usually require some specific combination of temperature and pressure. Forming is accomplished by clamping a sheet of superplastic material into a die and subsequently applying differential gas pressure to form the sheet to the die at a specified temperature. This temperature for aluminum is typically around 450°C to 500°C. [3] A schematic illustrating the process is shown in Figure 2. [6]
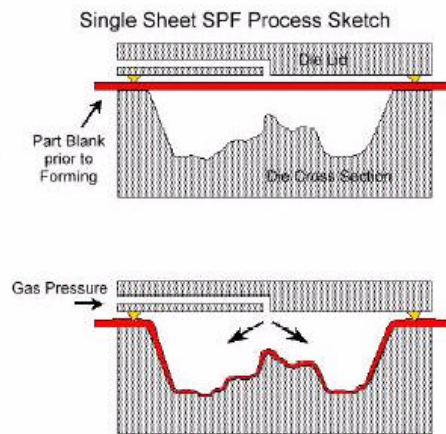
Figure 2.   Schematic representation of the superplastic forming process [6]

2. Prerequisites for Superplastic Forming

Not every material can be formed superplastically; there are several known requirements. Fine, equiaxed grains are required, no larger than ten microns in diameter. In addition, high-angle boundaries are necessary to facilitate grain boundary sliding. A predominance of high-angle boundaries is typically found in materials with random grain orientations, although such boundaries are often associated with certain texture components in materials with preferred orientations. In addition, in order to preclude

3

grain growth, it is often necessary to have a fine distribution of second phase particles to inhibit grain boundary migration. [2,7-9]

B. MECHANISMS OF SUPERPLASTICITY

The constitutive equation for material flow behavior is seen in Equation 1. [1]

$$\boldsymbol{s} = k\dot{\boldsymbol{e}}^{m} \tag{1}$$

$$\text{where } \boldsymbol{s} \quad = \text{true flow stress}$$
$$k \quad = \text{material constant}$$
$$\dot{\boldsymbol{e}} \quad = \text{true strain rate}$$
$$m \quad = \text{strain-rate-sensitivity coefficient}$$

Typical materials deforming plastically exhibit a strain-rate-sensitivity coefficient of less than 0.2, whereas Newtonian viscous materials have a value of 1. Materials undergoing superplastic deformation will typically exhibit m values greater than 0.33. [1] The strain-rate-sensitivity coefficient is directly related to the stress exponent: $n = 1/m$. The lower the value of the stress exponent (n), the more sensitive the flow stress of the material is to changes in strain rate (m).

There are two independent mechanisms in superplasticity: grain boundary sliding and dislocation creep. These two mechanisms are independent and therefore additive; the faster of the two mechanisms will dominate deformation. [9]

1. Grain Boundary Sliding (GBS)

Grain boundary sliding accommodated by slip or diffusional flow and occurs along the grain boundaries and in the mantle-like regions of the grain. The constitutive equation is seen in Equation 2. [2,4]

$$\dot{\boldsymbol{e}}_{GBS} = AD_{eff}^{*}\left(\frac{1}{\overline{L}}\right)^{2}\left(\frac{\boldsymbol{s}}{E}\right)^{n} \tag{2}$$

where $\dot{\boldsymbol{e}}_{GBS}$ = strain rate due to grain boundary sliding

A   = material constant

D_{eff}^{*} = effective coefficient of diffusivity

$\overline{L}$ = linear mean intercept grain size

$\boldsymbol{s}$ = true stress

E   = Young's modulus

n   = stress exponent, 2

With the application of a tensile stress, diffusion occurs along the grain boundaries as grain boundary interfaces slide past each other. Because this process occurs along the grain boundaries, there is a strong dependence on the grain size as seen in the constitutive equation. In addition, because the process is occurring at the grain boundaries, entire grains are rotating. This typically results in the grains remaining equiaxed and random in texture. [8]

2.   Dislocation Creep

Dislocation creep occurs through slip and climb within the grain interior, or core. The climb process requires diffusion. The equation governing dislocation creep is given by Equation 3. [4]

$$\dot{\boldsymbol{e}}_{disl} = KD \left(\frac{\boldsymbol{s}}{E} \right)^{n} \tag{3}$$

where $\dot{\boldsymbol{e}}_{disl}$ = strain rate due to dislocation creep

K   = material constant

D   = lattice coefficient of diffusivity

$\boldsymbol{s}$ = true stress

E   = Young's modulus

n   = stress exponent, typically 3 - 5

Whereas in grain boundary sliding entire grains rotate randomly in space, when a material is subjected to a tensile stress in dislocation creep, the lattice within the grain rotates in certain characteristic patterns because of the glide and climb. This results in grain elongation and the development of a preferential orientation or texture. Grain size is expected to have no effect on diffusional creep because the glide and climb processes occur within the grain. [9]

3.   Superplastic Deformation

The sum of the two independent mechanisms characterizing superplastic deformation is seen in Equation 5.

$$\dot{\boldsymbol{e}}_{SP} = \dot{\boldsymbol{e}}_{GBS} + \dot{\boldsymbol{e}}_{disl} = AD_{eff}^{*}\left(\frac{1}{\overline{L}}\right)^{2}\left(\frac{\boldsymbol{s}}{E}\right)^{n} + KD\left(\frac{\boldsymbol{s}}{E}\right)^{n} \tag{4}$$

Figure 3 shows a schematic representation of Equations 2, 3, and 4. [4] The intersection of the grain boundary sliding curve (Equation 2) with the dislocation creep curve (Equation 3) is the transition region between the mechanisms. The dominant mechanism in superplastic deformation (Equation 4) is grain boundary sliding until the transition region, where dislocation creep begins to dominate.
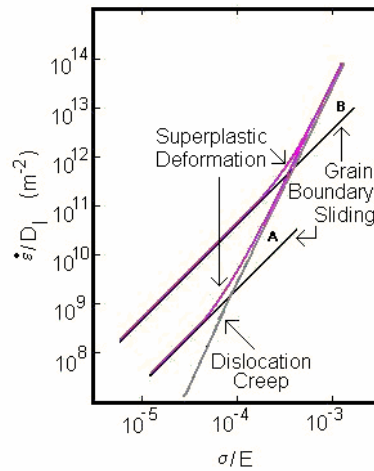
Figure 3.   Schematic representation of superplastic deformation and its constitutive mechanisms (adapted from [4])

One important feature of the curves in Figure 3 is the slope. The slope n is directly related to the material's resistance to necking. It is desirable for the material to neck as little as possible because necking leads to non-uniform thinning and possible failure; it is thus preferred to have as shallow a slope as possible (low n value). In the grain boundary sliding regime, the value for n is two while for dislocation creep it ranges from three to five. Therefore, it is desirable to remain in the grain boundary sliding regime as long as possible. [1,2,10]

One way of keeping deformation in the grain boundary sliding regime is to decrease the grain size. Since grain boundary sliding is dependent on grain size, a decrease in grain size will shift the grain boundary sliding curve up, as seen in Figure 3. As the grain size is decreased (shifting from curve A to B), the transition between mechanisms is shifted to the right and composite curve follows the grain boundary sliding curve to higher values of diffusion-compensated strain rates, $\dot{e}/D_l$. Thus, for a given stress, the strain rate is increased or, in a practical sense, this allows for an increase in strain rate while keeping the resistance to necking the same and reducing the effective stress. Industrially applied, this would lead to faster forming times.

C. ALUMINUM ALLOY 5083

AA5083 is a moderate strength aluminum alloyed primarily with magnesium and manganese. Table 1 shows the nominal composition of AA5083. [11] The combination of alloying elements provides for good corrosion resistance and result in a formable, weldable alloy. [3] AA5083 is an engineering alloy; in addition to intentional alloying elements, other elements remain from the manufacturing process. The cost to purify the alloy would drive the price of the material up, rendering it no longer cost effective for manufacturing use.

Table 1.   Nominal composition of AA5083 [11]

Element	Weight %
Al	Bal.
Mg	4.0 – 4.9
Mn	0.40 – 1.0
Cr	0.05 – 0.25
Cu	= 0.10
Fe	= 0.40
Si	0.40 - 0.70
Ti	= 0.15
Zn	= 0.25
Others	= 0.15

AA5083 can be processed superplastically.   However, grain sizes typically average eight microns. [12] For forming purposes, this gives only marginal performance. Though it is desired to reduce the grain size, current methods to predict grain size are generally empirical in nature and limited in scope. The purpose of this research is to develop a way of predictably refining the grain size.

As industry attempts to move from the direct-chill (DC) to continuously cast (CC) methods, it is important to limit the amount of cold rolling imparted into the material. This is important for several reasons. First, cold rolling is a high-energy-input process. The more cold-roll strain imparted into the material, the harder it becomes to deform the material, and, in turn, the more energy that is required for processing. The final thickness of the cast product is directly related to both how quickly the cast product can be produced and how much cold-rolling strain can be imparted in the material. The thinner the finished cast product, the less cold roll strain can be imparted. (Cold-rolling strain is related to thickness ratios.) However, thinner cast products can be produced much faster because they cool quicker. Therefore, not only would it be beneficial to put in less cold-rolling strain because it is a high-energy input process, but also because it would allow for quicker production of the material. [13]

D.   ANNEALING

1.   The Process

In a non-heat treatable alloy such as AA5083, the only technique of controlling grain size is through recrystallization by deformation and annealing. When a material is cold worked, large grains are elongated as input strain energy is stored in defects such as vacancies, dislocations, and stacking faults. This higher state of internal energy is thermodynamically unstable, however there is an energy barrier preventing the spontaneous release of this stored strain energy. Annealing provides the necessary thermal activation energy to overcome this energy barrier and return to a lower state of internal energy. [14] With the addition of heat and the passage of time, new strain-free grains will continue to grow until they have completely overtaken the deformed matrix. These new grains will typically be smaller than the original grains prior to the onset of deformation. Figure 4 shows a schematic representation of the annealing process.
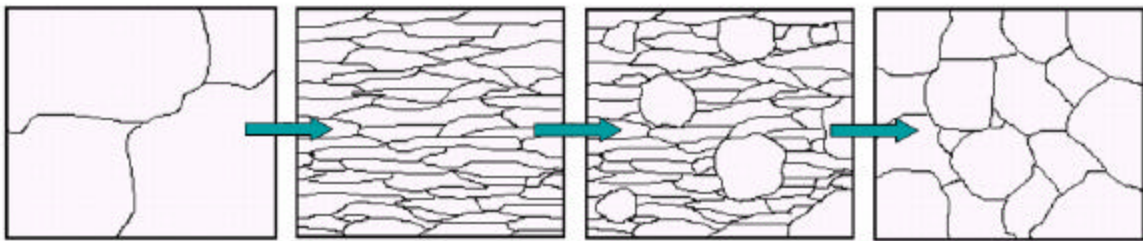
Figure 4.   Schematic representation of the annealing process

Annealing involves recovery, recrystallization, and grain growth. However, since recrystallization is the primary interest in this research, the recovery and grain growth stages will be only briefly discussed, followed by a more in-depth treatment of recrystallization mechanisms.

2. Recovery

During recovery, the thermal activation is great enough to allow for point defects to be annealed out and for dislocations to rearrange or annihilate one another. A limited amount of strain energy is released providing some softening; however, there is not enough input energy to allow for the migration of high-angle boundaries. This precludes the formation of nuclei of new, strain-free grains. [14]

3. Recrystallization

There are two stages to recrystallization commonly known as primary and secondary recrystallization. During primary recrystallization, the new, strain-free grains begin to nucleate. Secondary recrystallization is marked by the growth of these nuclei. Primary and secondary nucleation occur concurrently and the driving force for both is the release of the stored strain energy. [14] This stage requires a greater amount of activation energy due to the motion of high-angle boundaries. This will be discussed in the next section.

4. Grain Growth

Grain growth is the last stage in the recrystallization process. Once the deformed matrix has been replaced by the strain-free grains, grain boundaries migrate towards their center of curvature. Because this is a constant volume process, smaller grains are consumed at the expense of larger grains. The driving force for grain growth is different from secondary recrystallization. Once the entire deformed matrix has been replaced with the strain-free grains, the driving force can no longer be the release of strain energy. Instead, the driving force for grain growth is the reduction of grain boundary free energy. This is a substantially smaller driving force than that for recrystallization. [14]

E.   MECHANISMS OF RECRYS TALLIZATION

The precise mechanisms of recrystallization have not been well established. There are many theories as to how nucleation occurs. It is agreed that nucleation does not happen through atom-by-atom addition to form the stable nucleus. The amount of energy necessary for nuclei to form a critical size and subsequently grow is so large that, even at temperatures close to melting where lattice diffusion is the fastest, essentially no nucleation is predicted. In practice, nucleation and growth occurs, thus it must not happen in this manner. [14] Instead, it is predicted that nucleation occurs at areas of higher stored energy so that the required activation energy is less. These sites are typically small in volume and highly disordered. In addition to lower activation energy, less growth is required for high-angle boundaries to form with the matrix. Examples of these sites are previous grain boundaries, boundaries of deformation bands, intersections of mechanical twins, or second phase particles. [14]

One theory as to how nucleation occurs is illustrated in Figure 5. At the onset of deformation, the grain subdivides into cells and subgrains. The cells are the smallest divisions of the grain. They remain equiaxed and are separated from each other by low-angle boundaries. This means that the lattice rotation between the two is small (less than 15°) and there is only a small amount of disorder at those boundaries. These low-angle boundaries are difficult to move because of lattice registry. [7] A small group of cells together form a subgrain. The subgrains are typically elongated and, unlike the cells, they are separated by high-angle boundaries (15° or greater).   These high-angle boundaries form preferential sites for nucleation because of the high energy due to the large amounts of disorder. In addition, it is 100 to 1,000 times easier for a high-angle boundary to move. In order for the nuclei to grow, it is necessary for the boundaries to migrate. [16,17] Other theories of recrystallization mechanisms exist; examples of some of the theories are described in detail in References 15 and 18-21.
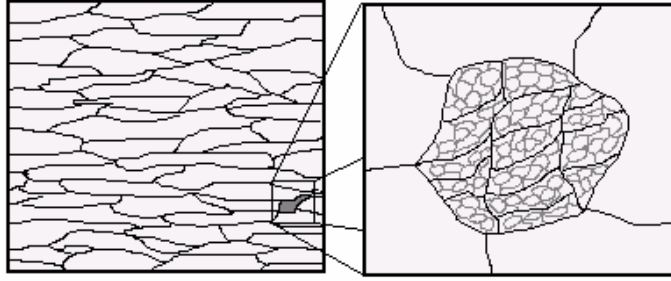
Figure 5.   Schematic showing the subdivision of a grain due to deformation

The grain growth during secondary recrystallization is due to the migration of high-angle boundaries. Barriers such as a fine dispersion of second phase particles can inhibit high-angle boundary migration. Thus, even if these particles do not serve as site for nucleation, they can aid in refining grain size by preventing grain growth during recrystallization. [1,2,7,8,14,22,23]

F.   PARTICLE STIMULATED NUCLEATION (PSN)

As discussed earlier, second phase particles can serve as sites for nucleation because of the increased local dislocation density required for accommodation of the particles. Humphreys developed particle stimulated nucleation theory to predict the resulting grain size in a dilute aluminum-silicon alloy.

Humphreys developed a mathematical model to predict the grain size given a specific volume fraction of particles and a particular amount of cold-rolling strain. [24] Knowing the amount of strain, the dislocation density field around the particle can be predicted. In order for the second phase particle to serve as a nucleation site, there is a certain amount of energy (disorder) that is required for a stable nucleus to form and grow. If the magnitude of the dislocation density can be determined knowing the cold-rolling strain, than the critical particle size for nucleation can be determined. This is illustrated schematically in Figure 6. [25]
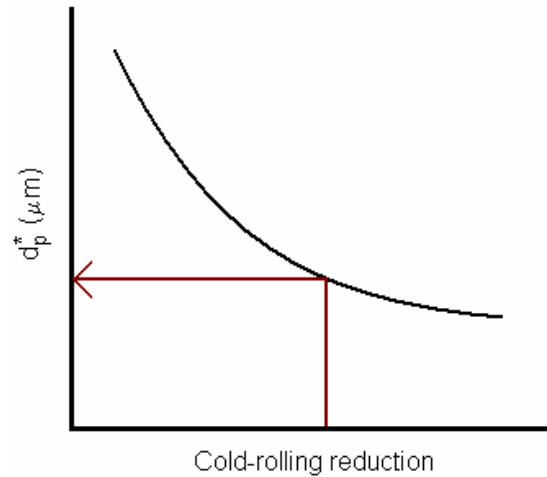
Figure 6.   Schematic representation of the determination of the critical particle size for nucleation given the cold-rolling reduction (adapted from [25])

Once a critical particle size is determined, this information can be combined with the volume fraction of the particles to determine the grain size. (Figure 7) [25] Determination of grain size assumes that the diameter of the grain is equal to half of the spacing in between the particles.
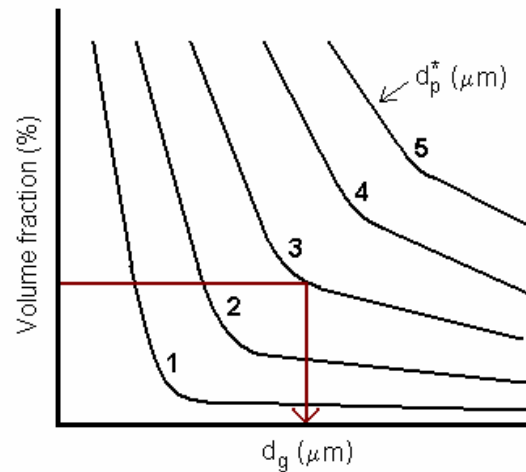
Figure 7.   Schematic representation of the determination of grain size given the critical particle size and the volume fraction of the particles (adapted from [25])

Humphreys made several assumptions in his original theory. Not only did he assume that the grain size was half of the spacing between the particles, but he assumed

13

that the particles were of uniform size and had a uniform distribution. [24] This theory has proved to be sufficient for dilute, pure alloys, but may be insufficient for engineering alloys.

Instead of assuming particles of uniform size, second phase particle size distributions are modeled with a lognormal probability density function. Figure 8 is a representation of a particle size distribution modeled by a lognormal probability density function. The highlighted area under the curve represents all of the particles that would serve as nucleation sites given some critical particle size as suggested in Humphrey's original analysis.
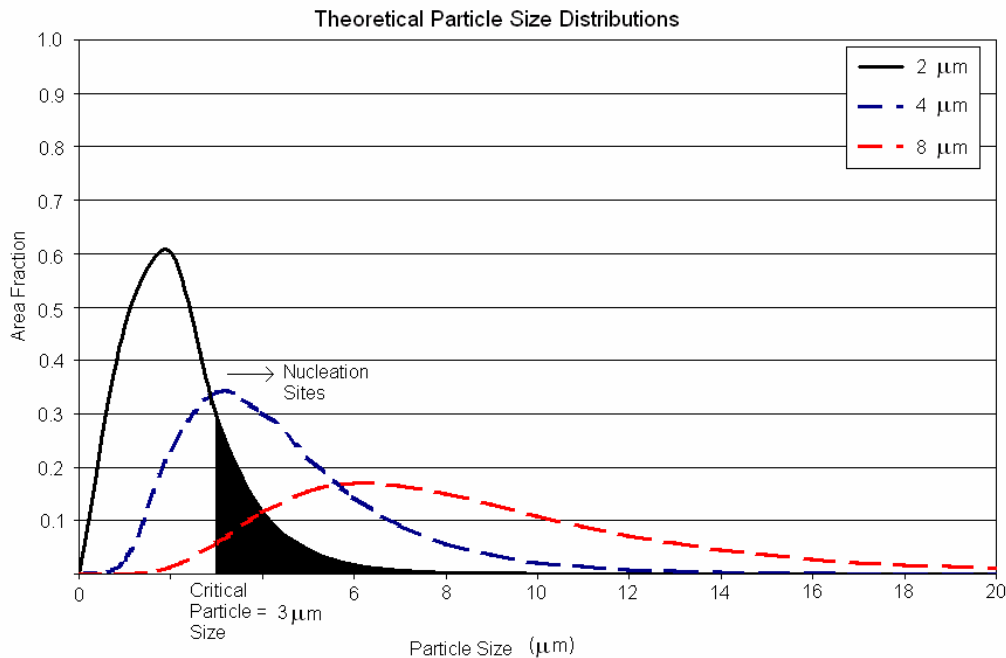
Figure 8.   Theoretical particle size distribution showing the PSN sites given a critical particle size

The dashed curves in Figure 8 illustrate what happens as the average of the particle size distribution is increased. Assuming that the critical particle size remains the same, the number of sites for nucleation increases for the assumed relationship between critical particle size and size distribution. This can be seen in Figure 9.

14
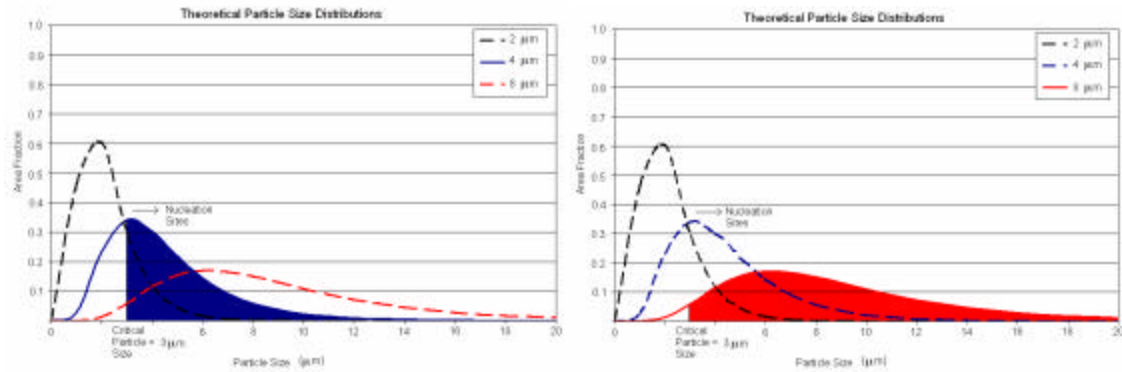
Figure 9.   Theoretical particle size distribution curves showing the increased number of PSN sites as the average particle size increases (same axes as Figure 8)

Examining these curves, it might be possible to conclude that it would be desirable to continue to increase the second phase particle average size as large as possible. However, this is not so. Assuming that all of the second phase has precipitated out of solution, the volume of the particles remains constant. Therefore, as some of the particles grow larger, smaller particles are consumed. This results in increasing average spacing between the particles. This is illustrated schematically in Figure 10.
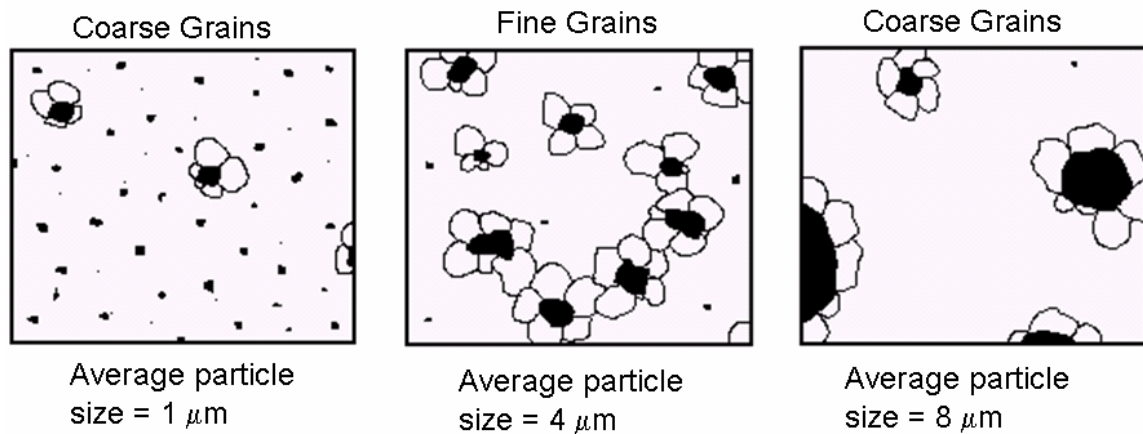
Figure 10.   Schematic representation of the effect of increasing the average particle size on the resulting grain size

Figure 10 shows what effectively happens with the theoretical particle size distributions from Figure 8. As the average particle size increases, the number of sites

for nucleation increases. However, as the particle size increases, the spacing in between the particles also increases. This suggests some optimal particle size where a sufficient number of particles are serving as nucleation sites, but the particles remain spaced closely enough to result in a fine grain size.

III. EXPERIMENTAL PROCEDURES

A. PURPOSE OF RESEARCH

Current processing techniques and their effects on grain size are empirical in nature. The goal of many researchers is to be able to more precisely determine the recrystallization mechanisms and thus the grain size. [2,8,10] Using the knowledge of particle stimulated nucleation, AA5083, and previous experience with thermomechanical treatments, the goal of this research is to develop a method to predictably refine the grain size.

B. THERMOMECHANICAL PROCESSING TECHNIQUES

1. As-cast Material

The material, manufactured by direct-chill casting, was received in the as-cast condition. Table 2 shows the results of chemical analysis of the billet material, in agreement with the composition tolerances for the AA5083 composition. [11]

Table 2. Composition of tested AA5083 [11]

Element	Weight % (tested)	Weight % (nominal)
Al	Bal.	Bal.
Mg	4.88	4.0 – 4.9
Mn	0.80	0.40 – 1.0
Cr	0.10	0.05 – 0.25
Cu	0.03	= 0.10
Fe	0.21	= 0.40
Si	0.08	= 0.40
Ti	0.007	= 0.15
Zn	0.008	= 0.25
Others	= 0.15	= 0.15

Figure 11 shows the composite schematic representing each stage of the thermomechanical processes given to the as-cast material. Subsequently, each stage will be discussed and the effect that ideally it has on the microstructure.
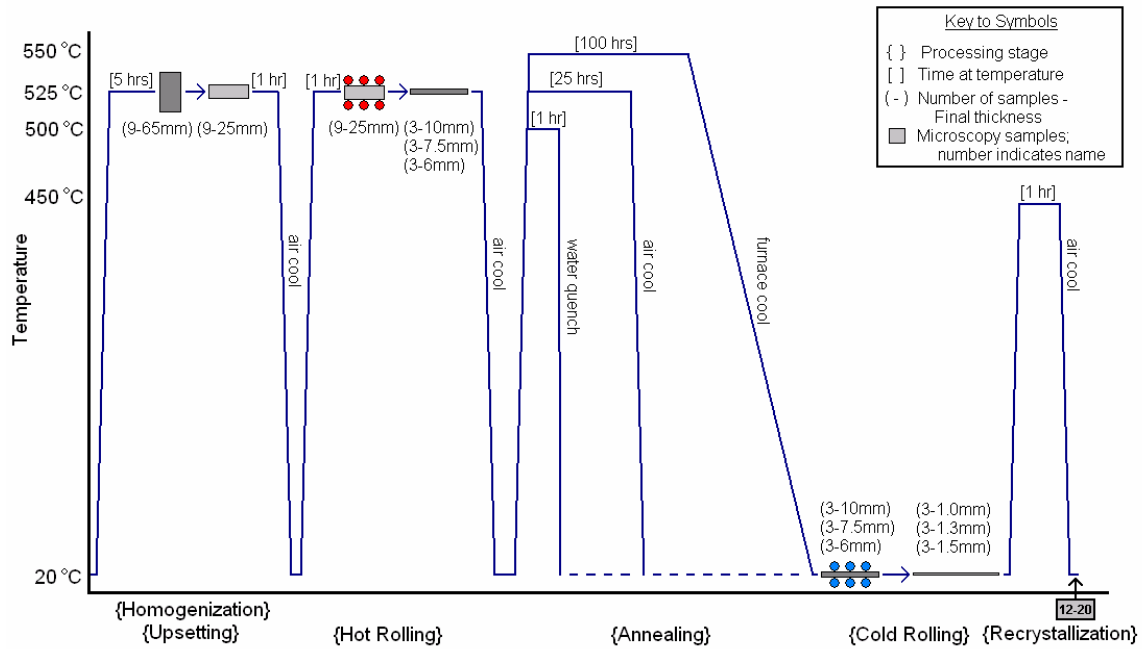
Figure 11.   TMT schematic of processing history

2.   Homogenization and Upsetting
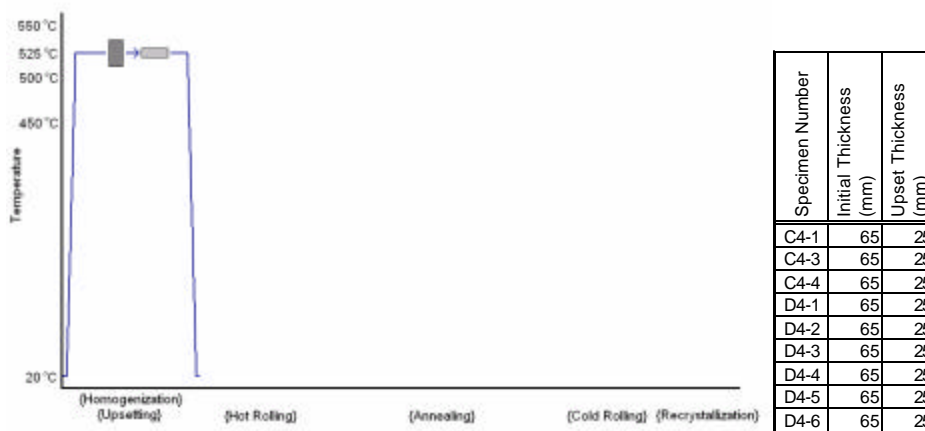
Figure 12.   TMT schematic and specimen information for homogenization and upsetting

The first stage in the TMT is an extended annealing treatment at 525°C for five hours (Figure 12). The purpose of this is to homogenize the material. After casting, often times there are micro-segregation effects due to the different cooling ranges of elements, phases, and intermetallic compounds. Holding the material at an elevated temperature for an extended amount of time encourages diffusion within the material and thus allows for the segregation effects to be reduced. [14,26]

In order to fit the material into the rolling mill, the height of the specimen had to be reduced from 65mm to 25mm. Immediately after the 5-hour annealing treatment, the samples were removed quickly from the furnace, placed between two heated, lubricated platens, heated to 525°C, and upset at a constant cross-head rate of 25mm/min. Immediately after reaching their final height, the specimens were removed from the platens and placed back into the furnace for another hour and then allowed to air cool.

3. Hot Rolling

Specimen Number	Initial Thickness (mm)	Upset Thickness (mm)	Hot Rolled Thickness (mm)
C4-1	65	25	10
C4-3	65	25	10
C4-4	65	25	10
D4-1	65	25	7.5
D4-2	65	25	7.5
D4-3	65	25	7.5
D4-4	65	25	6
D4-5	65	25	6
D4-6	65	25	6
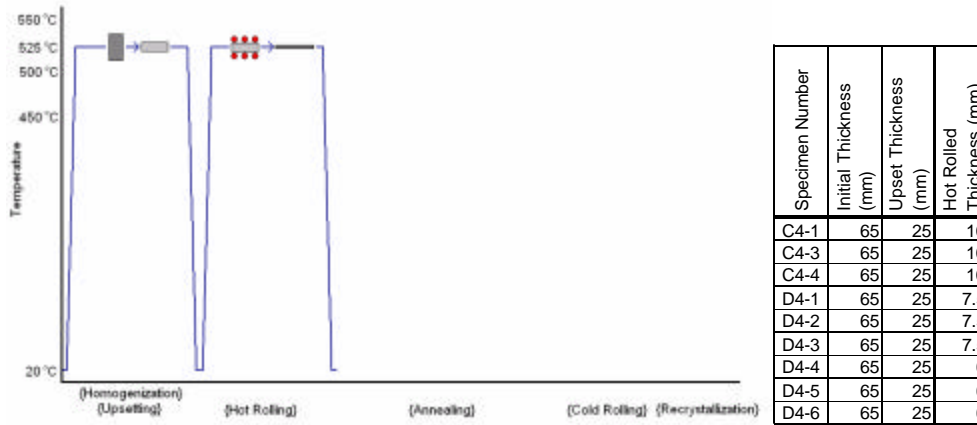
Figure 13.   TMT schematic and specimen information for hot rolling

Hot rolling (Figure 13) was performed to further break up the as-cast microstructure. The sections were brought to temperature for one hour and hot rolled with reheating and measurement between passes. All sections of the same thickness were rolled concurrently to standardize the procedure as much as possible. In between rolling passes, samples were placed back in the furnace for 10 minutes. Thicknesses were

reduced at 10% per rolling pass. Final thicknesses were determined by the amount of cold work desired in subsequent cold rolling.

4. Annealing

Specimen Number	Initial Thickness (mm)	Upset Thickness (mm)	Hot Rolled Thickness (mm)	Anneal Time (hr)	Anneal Temperature (°C)
C4-1	65	25	10	100	550
C4-3	65	25	10	25	525
C4-4	65	25	10	1	500
D4-1	65	25	7.5	100	550
D4-2	65	25	7.5	25	525
D4-3	65	25	7.5	1	500
D4-4	65	25	6	100	550
D4-5	65	25	6	25	525
D4-6	65	25	6	1	500
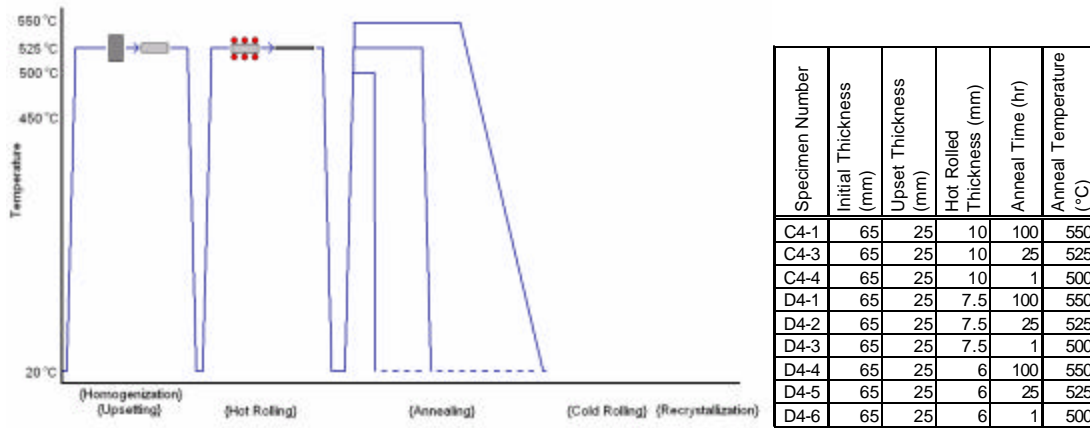
Figure 14.   TMT schematic and specimen information for annealing

The annealing phase of the thermomechanical cycle was intended to serve as a solution heat treatment for the alloy. As seen in Figure 14, three separate heat treatments were performed. Each treatment was designed to produce different particle distributions. The purpose of the lowest temperature, shortest time, and fastest cool was to produce the smallest mean particle size, whereas the highest temperature, longest time, and slowest cooling would produce the largest mean particle size. The theoretical particle size distributions intended to be produced by the annealing treatments are illustrated in Figure 15.
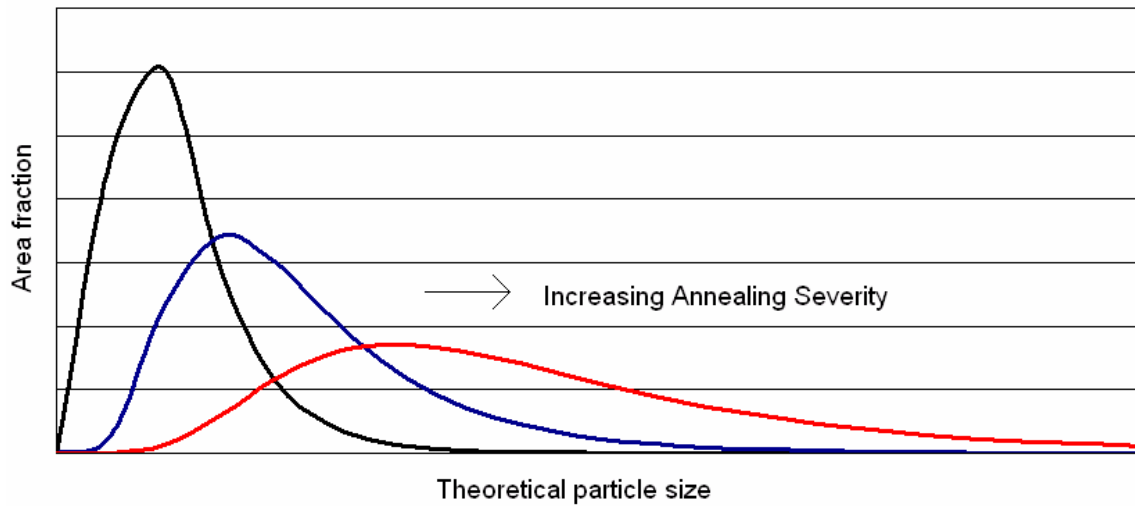
Figure 15.   Theoretical particle size distributions following annealing

The temperatures chosen were based on the phase diagrams as seen in Figure 16. [27] The binary aluminum-magnesium and aluminum-manganese phase diagrams can be used separately to approximate the behavior of the AA5083 because there are no ternary aluminum-magnesium-manganese phases in this system. It was desired to get all the particles from casting to return into solution by raising the temperature above the solvus temperature. In the aluminum-manganese diagram, it is evident that the solvus temperature is around 650°C for 0.8 weight percent manganese. Looking at the aluminum-magnesium diagram, 650°C is well above the solidus temperature of the alloy. In order to avoid melting the material, the maximum annealing temperature was chosen just below the solidus temperature on the aluminum-magnesium phase diagram. Since this is well above the solvus line, it was expected that all of the magnesium would return into solution and subsequent precipitation of aluminum-magnesium phases could be controlled through cooling. The aluminum-manganese particles would not completely go back into solution since the temperatures are below their solvus line. It was anticipated that the existing particles would coarsen with the annealing treatment. The three temperatures chosen are shown as the points on each phase diagram.
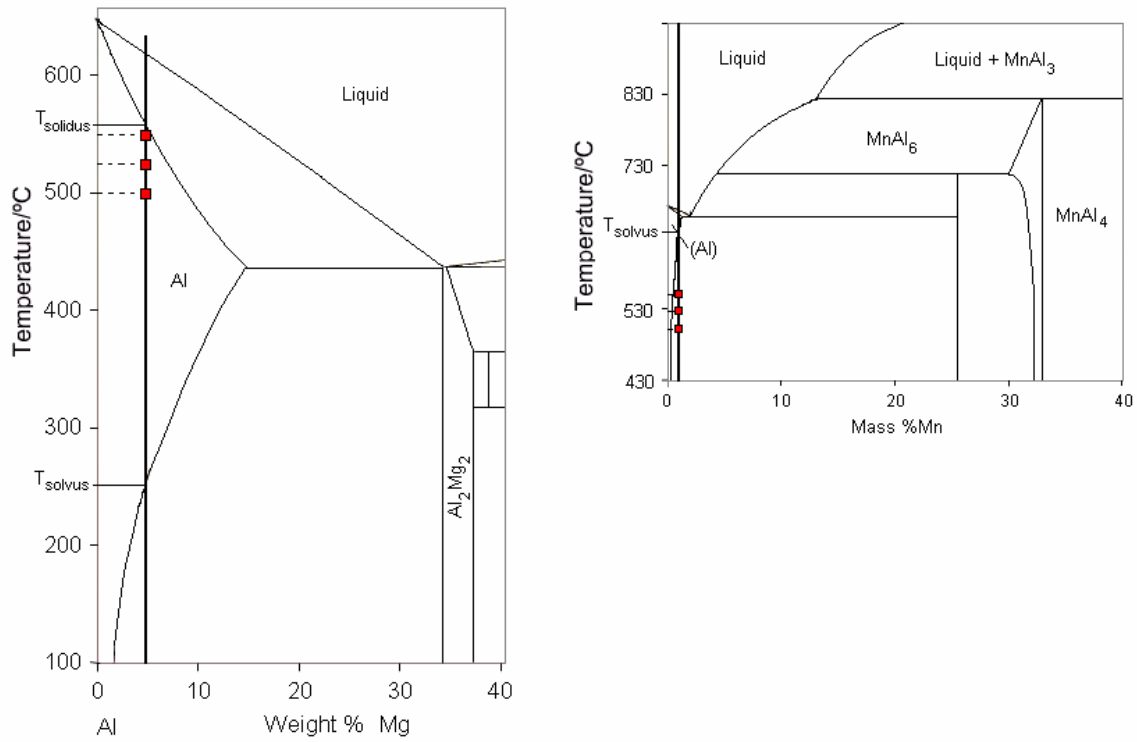
Figure 16.   Phase diagrams for Al-Mg and Al-Mn binary systems (Adapted from [27])

5.   Cold Rolling

Specimen Number	Initial Thickness (mm)	Upset Thickness (mm)	Hot Rolled Thickness (mm)	Anneal Time (hr)	Anneal Temperature (°C)	Cold Rolled Thickness (mm)
C4-1	65	25	10	100	550	1
C4-3	65	25	10	25	525	1
C4-4	65	25	10	1	500	1
D4-1	65	25	7.5	100	550	1.3
D4-2	65	25	7.5	25	525	1.3
D4-3	65	25	7.5	1	500	1.3
D4-4	65	25	6	100	550	1.5
D4-5	65	25	6	25	525	1.5
D4-6	65	25	6	1	500	1.5
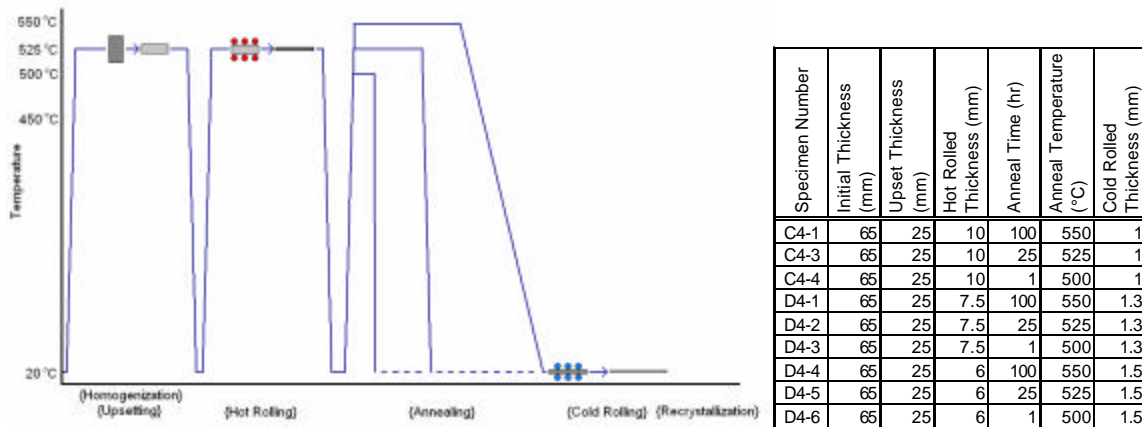
Figure 17.   TMT schematic and specimen information for cold rolling

Particle stimulated nucleation theory also suggests that increasing the input strain will have an effect on the critical particle size. The cold rolling part of the process served to vary the amount of strain (Figure 17), thus resulting in a reduction in the critical particle size. If the critical particle size is decreased, more particles will serve as nucleation sites. This is shown theoretically in Figure 18; as the critical particle size shifts to the left, the area under the curve to the right of the critical particle size increases. It is important to note that Figure 18 is a theoretical representation of what is anticipated by combining both the annealing and strain effects.
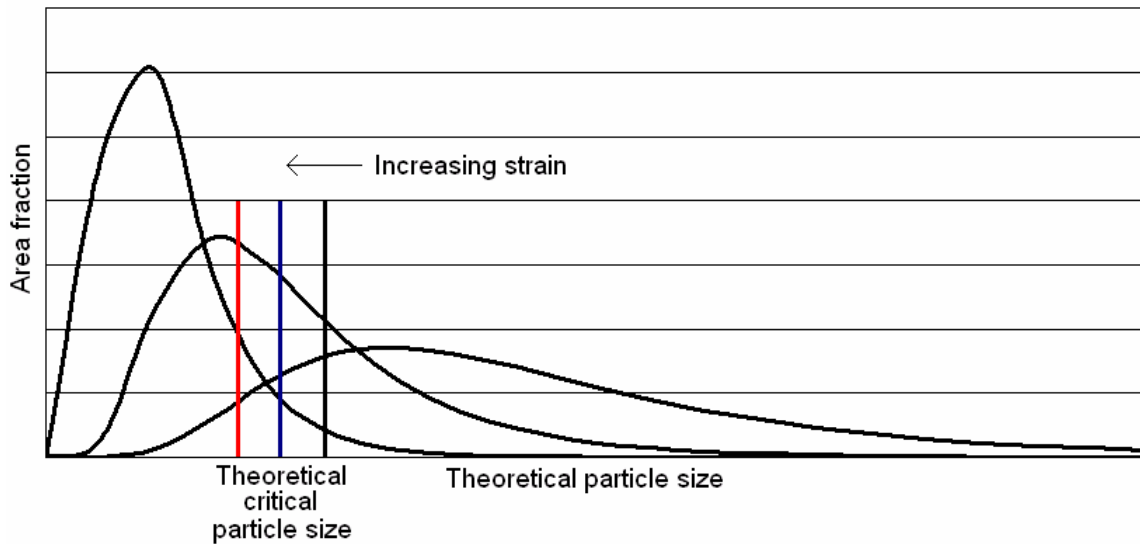
Figure 18.   Theoretical impact of increasing the strain on various particle distributions

6.   Recrystallization
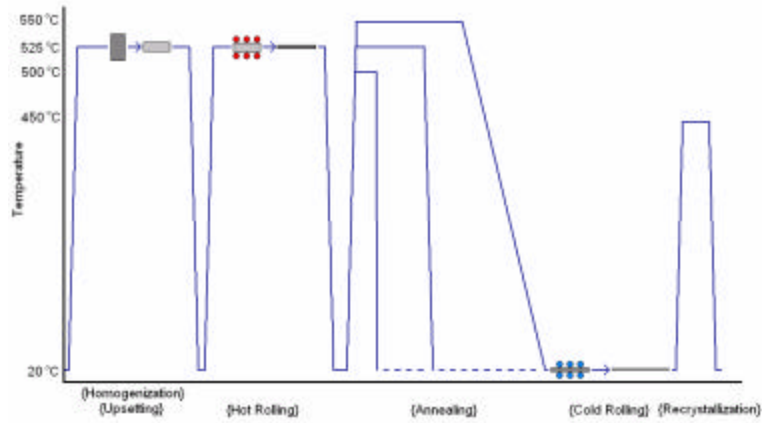
Specimen Number	Initial Thickness (mm)	Upset Thickness (mm)	Hot Rolled Thickness (mm)	Anneal Time (hr)	Anneal Temperature (°C)	Cold Rolled Thickness (mm)	Recrystalization Time (hr)	Recrystallization Temperature(°C)
C4-1	65	25	10	100	550	1	1	450
C4-3	65	25	10	25	525	1	1	450
C4-4	65	25	10	1	500	1	1	450
D4-1	65	25	7.5	100	550	1.3	1	450
D4-2	65	25	7.5	25	525	1.3	1	450
D4-3	65	25	7.5	1	500	1.3	1	450
D4-4	65	25	6	100	550	1.5	1	450
D4-5	65	25	6	25	525	1.5	1	450
D4-6	65	25	6	1	500	1.5	1	450

Figure 19.   TMT schematic and specimen information for recrystallization treatment

Upon the completion of cold rolling, small sections were removed from each specimen from the same relative location for a recrystallization study.   These nine samples were treated as shown in Figure 19. These samples were the primary focus of the study.

C. RECRYSTALLIZATION STUDY

1. Sample Preparation

Samples for the recrystallization study were removed from the specimen by electrical discharge machining (EDM) and a high speed diamond wafering blade. Sample preparation was then performed in accordance with standard metallographic techniques as described in Reference [14]. Table 3 summarizes the steps used in preparation. Both grinding and polishing were done with light pressure in an attempt to avoid tearing out particles from the soft aluminum matrix. Samples prepared for SEM work were electropolished to produce a strain-free surface.

Table 3.   Summary of sample preparation techniques

Grinding					
500-grit	Water lubricant	4 min.*	100 RPM	Light pressure
Ethanol rinse					
1000-grit	Water lubricant	2 min.**	100 RPM	Light pressure
Ethanol rinse					
2400-grit	Water lubricant	2 min.**	100 RPM	Light pressure
Ethanol rinse					
4000-grit	Water lubricant	2 min.**	100 RPM	Light pressure
Ethanol rinse					
Ultrasonic Cleaning	Ethanol	10 min.		
Polish					
Buhler MICROCLOTH	3 μm Metadi diamond suspension	10 min.	50 RPM	Light pressure
Ultrasonic Cleaning	Ethanol	10 min.		
Buhler MICROCLOTH	1 μm Metadi diamond suspension	10 min.	50 RPM	Light pressure
Ultrasonic Cleaning	Ethanol	10 min.		
Buhler MICROCLOTH	0.05 μm Colliodal silica suspension	10 min.	50 RPM	Light pressure
Ultrasonic Cleaning	Ethanol	10 min.		
Electropolish					
20% $HClO_4$, 70%C_2H_5OH, 10% Glycerol		20 sec.		20 volts
Ultrasonic Cleaning	Ethanol	10 min.		
* Until specimen is flat.					
** Until prior evidence of scratching is removed; rotated 90 degrees and repeated.					

2. Orientation Imaging Microscopy

Orientation imaging microscopy (OIM) was used as the primary method of data collection. OIM works in conjunction with scanning electron microscopy to determine

orientation data. Figure 20 shows a schematic representation of the configuration of the orientation imaging camera in the SEM chamber. [29] When an electron beam impinges on a crystalline solid, several types of emission result. One of these is a diffraction pattern, which is also known as a Kikuchi pattern. A sample set of a section of this diffraction pattern is shown in Figure 21. [29] A camera can then captures this pattern off of a phosphor screen for further analysis.
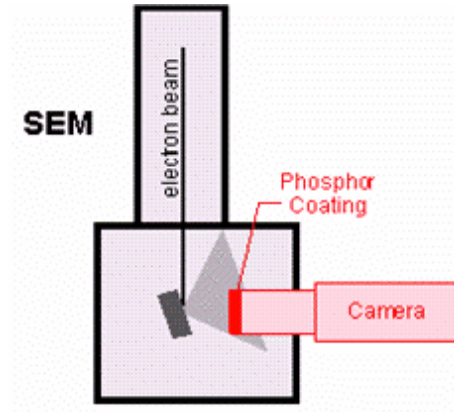
Figure 20.   Schematic representation of orientation imaging [29]
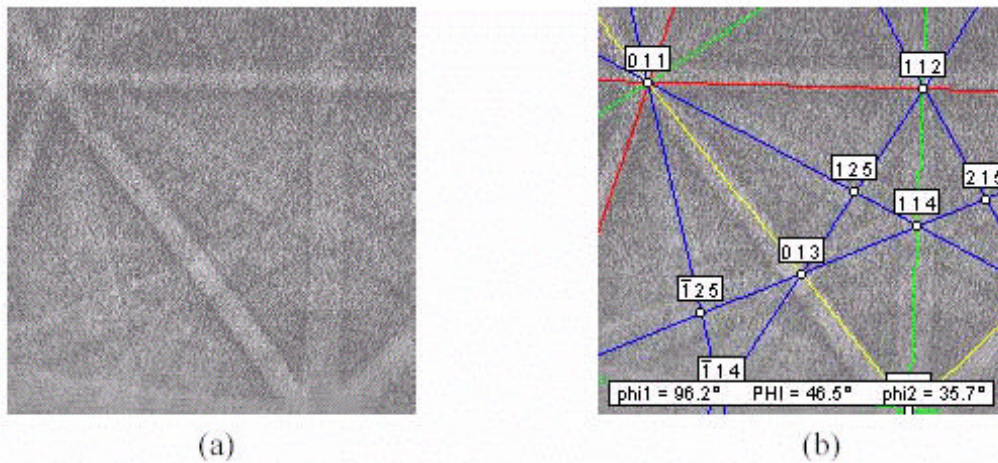
Figure 21.   Representation of (a) an image collected by OIM software and (b) a collected image with indexed pattern overlaid [29]

Each material has characteristic Kikuchi patterns that depend upon lattice type, atom spacing, and orientation. Samples of Kikuchi patterns are stored in a data base. The user inputs the primary type of material being investigated and the computer

compares the captured image with its reference image. Only a section of the pattern is captured by the camera as seen in Figure 20. By comparing the captured section to the reference, the computer assigns an orientation to the point, as exemplified in Figure 21. [29]

The orientations are described by three Euler angles. Figure 22 shows an example orientation of a grain in the rolled sheet. [30] The grain is represented by the cube with local axes x, y, and z. The three reference axes used are the rolling direction (RD), the transverse direction (TD), and the normal direction (ND). Each grain is rotated into the reference axes through three Euler rotations: a rotation about the z-axis (φ_1), a rotation about the x-axis (Φ), and another rotation about the z-axis (φ_2). This series of rotations is illustrated schematically in Figure 23. [30]
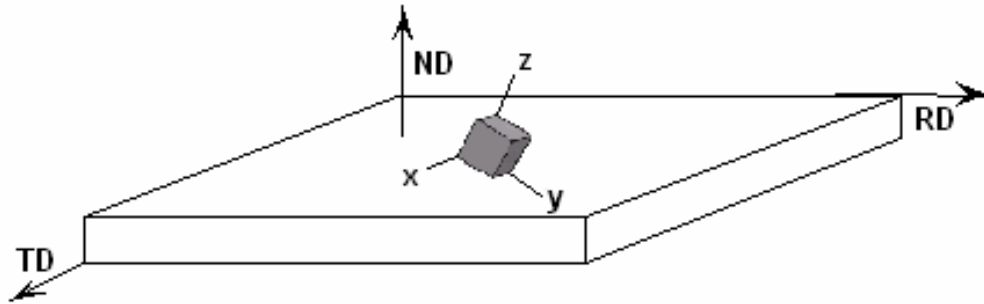
Figure 22.   Schematic representation showing labeling of local and reference axes (adapted from [30])
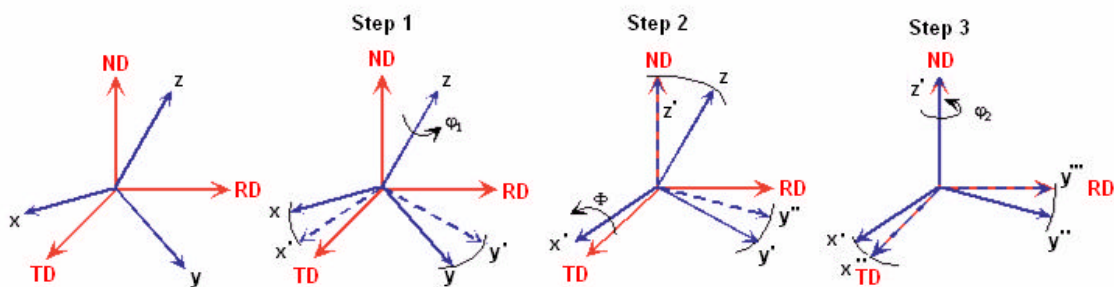
Figure 23.   Process of rotating axes to bring into coincidence (adapted from [30])

27

In order to complete a data set, the electron beam is caused to traverse the surface in a raster pattern as exemplified in Figure 24. At each point in the raster, several pieces of information are collected: the x- and y-coordinates of the point, the three Euler angles, a measure of image quality, and a confidence index. The image quality parameter describes the sharpness of the captured image. The confidence index is a measure of the confidence of the Euler angles; a confidence index greater than 0.10 means that probability of correct indexing is at least 95%. [29]
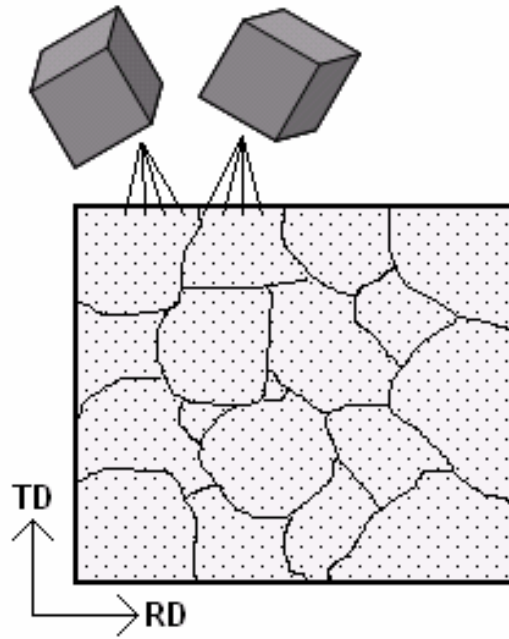
Figure 24. Schematic representation showing raster pattern over sample surface; example orientations shown for selected locations

These five measurements for each point on the raster pattern can be used to calculated a great deal of information about the sample. The information calculated which is useful in analysis of grain refinement is discussed briefly below.

D. ANALYSIS
1. Grain Maps

Grain maps are produced by the software using the image quality data. Image quality is a measure of the sharpness of the image captured by the camera. Typically

poor image quality measurements reflect either different phases (those phases not consisting primarily of the matrix element) or areas where the lattice is highly distorted. Such examples of poor image quality areas would be second phase particles and grain boundaries. The software can generate a map with the image quality for each data point measured that is representative of the grain structure. Overlaid on top of the image quality map are lines that represent different misorientations. The black lines indicate misorientations of 15° or greater (high-angle boundaries), whereas the white lines represent misorientations less than 15° (low-angle boundaries). An example of a generated grain map is seen in Figure 25.
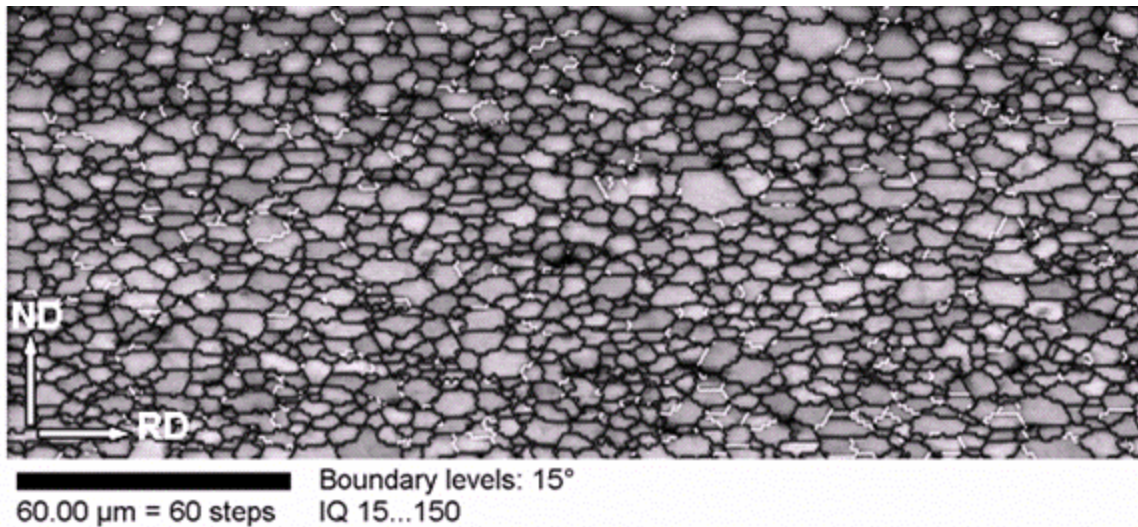
Figure 25.   Sample grain map constructed with image quality; misorientation lines overlaid
(=15° black, <15° white, 250 μm by 100 μm area, C4-1)

2.   Determination of Grain Size

As seen in Figure 25, grains in a specimen are not all of the same size. In order to represent the entire sample with one data point, some standardized representation needed to be chosen. The OIM software calculates grain size by counting the pixels with the same orientation. A circle with the same area is then fit to the pixels, and the grain diameter is taken as the diameter of that circle. [31]

The area weighted grain size was used due to its correlation to the linear mean intercept grain size which can be obtained through optical microscopy. The area-

weighted grain size is determined by multiplying each grain diameter by the corresponding grain area, summing for all grains, and dividing by the total area. The distribution of grain sizes was represented by histograms having bin widths of 1.0 micron and ranging from 1.0 to 18.0 microns. An example of a typical grain size distribution histogram is seen in Figure 26.

Representation of Grain Size Distribution (C4_1)
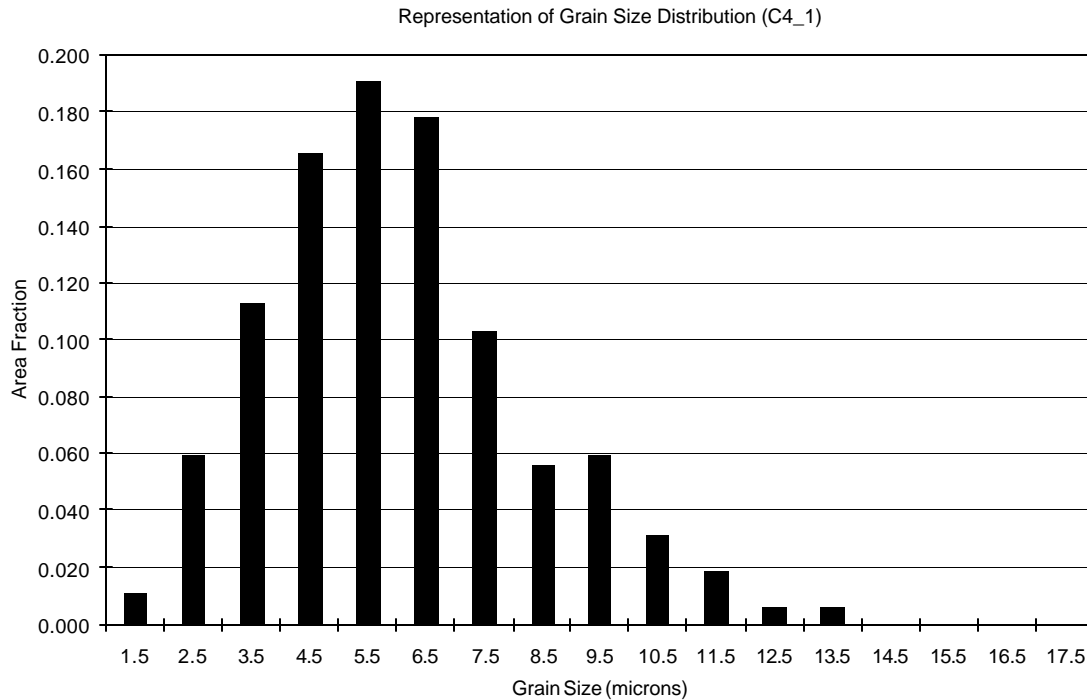
Figure 26. Example of a grain size distribution determined through orientation imaging (part of sample C4-1)

Several sets of data were collected for each of the nine samples. Prior to analysis, the data was cleaned and rotated. Cleaning of the data consisted of removing all the data points whose confidence index was lower than 0.10 (less than 95% confidence of correct orientation determination). The point was replaced with the same orientation as the majority of its neighbors. The data was subsequently rotated so that the microscope's default axes coincided with the actual axes of the sample.

The data sets were then evaluated to determine their quality. This was done on the basis of average confidence index and image quality as well as by observing the grain

map. Several sets of reliable data were taken for each of the nine samples. Grains that were cut off by the scan were excluded from analysis. In addition, only samples that contained over 500 grains were used in statistical analysis. Each sample had several grain size distribution histograms. A representative grain size distribution histogram was determined by combining all of the reliable data sets. In each data set, the total number of grains counted and the area fraction were used to determine the total number of grains per bin. The number of grains per bin per set was added, determining a total number of grains per bin in the entire sample set. A total area fraction was then determined using this number. Figure 27 shows a representation of the compiled data. Each bar represents a single data set calculated from the orientation imaging software. The line connects the dots which represent the combined data set at each interval.
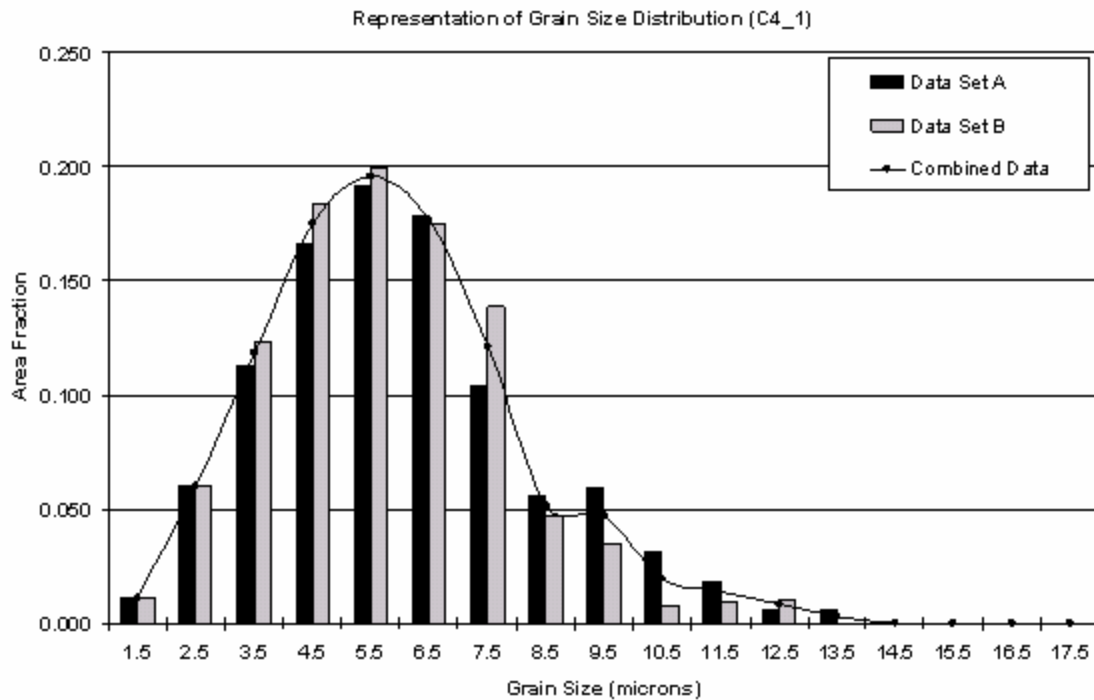
Figure 27.   Example of a few data sets for a single sample and their representative
distribution (part of sample C4-1)

3.   The Lognormal Distribution

In order to represent the histograms with some average value and associated error bars, a probably density function was fitted to the data. The probability density function chosen to represent the grain size data is the lognormal distribution.   Lognormal distributions are used frequently to describe growth and it is thus one of the most important distributions in nature. [32] Since grains nucleate and grow as do second phase particles, the lognormal distribution was also used to represent the grain size distribution.

The lognormal distribution was determined by fitting a normal distribution to the log of the grain size. The mean, central tendency, of the normal distribution of the log of the grain size was calculated using Equation 5.   In addition, the standard deviation (Equation 6) was calculated. [32,34]

$$m = \frac{\sum_{i=1}^{n} x_i}{n} \tag{5}$$

$$s = \sqrt{\frac{\sum_{i=1}^{n} (x_i - m)^2}{n-1}} \tag{6}$$

where n = sample size
x_i = log of grain size (diameter), log (d_g)
m = mean of normal distribution of log (d_g)
s = standard deviation of normal distribution of log (d_g)

These values can be directly converted into the mean and standard deviation of the lognormal distribution using Equations 7 and 8 respectively. Standard error was then calculated using Equation 9. [32-34]

$$a = 10^{\left(\frac{m^2}{\sqrt{s^2 + m^2}}\right)} \tag{7}$$

$$b = \sqrt{10^{\left(s/m\right)^2} + 1} \tag{8}$$

$$SE = \frac{b}{\sqrt{n}} \qquad (9)$$

where n   = sample size

           a   = mean of lognormal distribution of d_g

           b   = standard deviation of lognormal distribution of d_g

           m   = mean of normal distribution of log (d_g)

           s   = standard deviation of normal distribution of log (d_g)

           SE   = standard error of lognormal distribution

The lognormal distribution can be described by other attributes such as skewedness and shape factors, but these parameters were not analyzed in the subsequent investigation. An example of the lognormal distribution fit to the raw and compiled data is show in Figure 28.
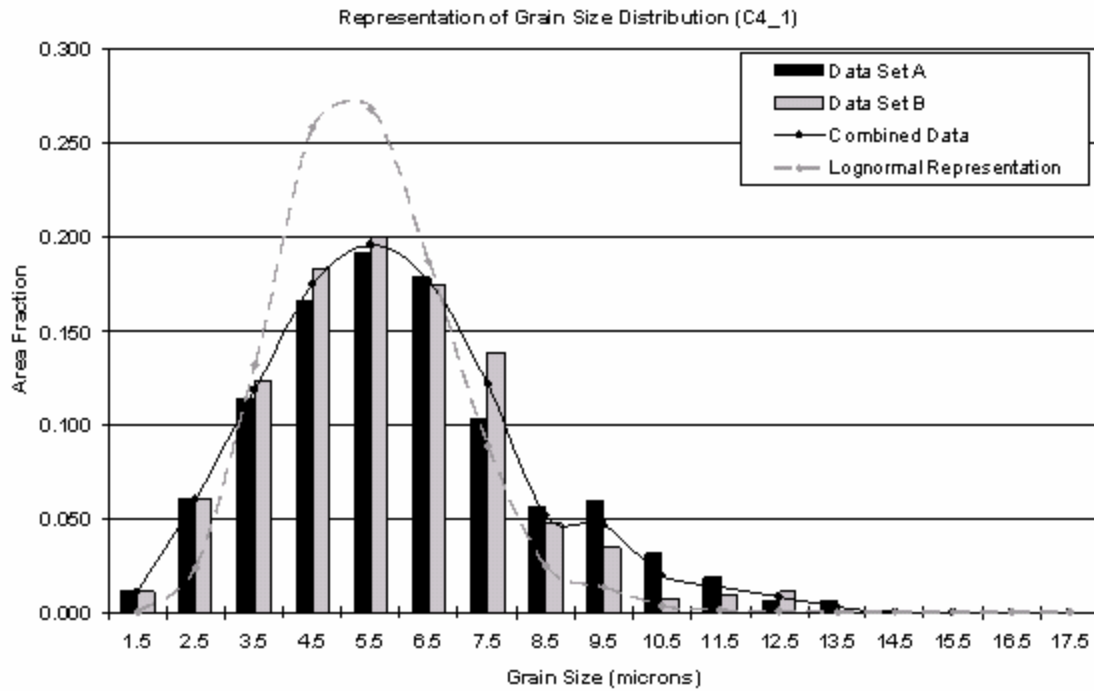
Figure 28.   Example of the lognormal distribution fit to the raw and compiled data (part of sample C4-1)

4. **Texture and Misorientation Angles**

Recrystallization can lead to the development of a preferred orientation. This texture is often related to, but not the same as, the deformation texture. For example, recrystallized aluminum that had been rolled often develops a texture with the {100} planes parallel to the RD-TD plane and the <001> direction parallel to the rolling direction. [9,14] Texture plots were generated for each data set to determine if a preferred orientation did exist in this sample set.

Misorientation is defined as the smallest angle required to bring a grain lattice into coincidence with the lattice of a neighboring grain. Because of cubic symmetry, the range of angles extends only from $0°$ to $62.8°$. The misorientation data was determined primarily to overlay onto the grain maps to differentiate between low and high-angle boundaries. However, histograms were also computed because a multi-component texture can lead to peaks in the misorientation histogram.

IV. RESULTS AND DISCUSSION

A. SAMPLE MATRIX

Table 4 shows a summary of the samples examined. Each of these samples were processed through the entire thermomechanical treatment as summarized in Figure 11.

Table 4.   Summary of prepared samples

Specimen Number	Initial Thickness (mm)	Upset Thickness (mm)	Hot Rolled Thickness (mm)	Anneal Time (hr)	Anneal Temperature (°C)	Cold Rolled Thickness (mm)	Recrystalization Time (hr)	Recrystalization Temperature(°C)	Cold Rolled Strain (in/in)
C4-1	65	25	10	100	550	1	1	450	2.30
C4-3	65	25	10	25	525	1	1	450	2.30
C4-4	65	25	10	1	500	1	1	450	2.30
D4-1	65	25	7.5	100	550	1.3	1	450	1.75
D4-2	65	25	7.5	25	525	1.3	1	450	1.75
D4-3	65	25	7.5	1	500	1.3	1	450	1.75
D4-4	65	25	6	100	550	1.5	1	450	1.39
D4-5	65	25	6	25	525	1.5	1	450	1.39
D4-6	65	25	6	1	500	1.5	1	450	1.39

B. EXAMPLES OF MICROSTRUCTURES AND TABULAR SUMMARY

Figure 29 contains two grain maps illustrating the extremes of the data. Table 5 summarizes the results obtained from all of the data sets collected. Each sample in Table 5 will be presented in figures represented by a single value of grain size with bars around the point representing one standard deviation.   The data point is the mean of the estimated lognormal distribution discussed earlier. The standard deviation bars are added as a reminder that the grain sizes are actually a range around the mean value. A measure of standard error was also determined. Standard error is the standard deviation of the total number of data points (in this case, all the grains counted). These values are not

shown in the figures as they are small in magnitude, particularly compared to the standard deviation. The lines connecting the data points show the trends of the mean for each condition.
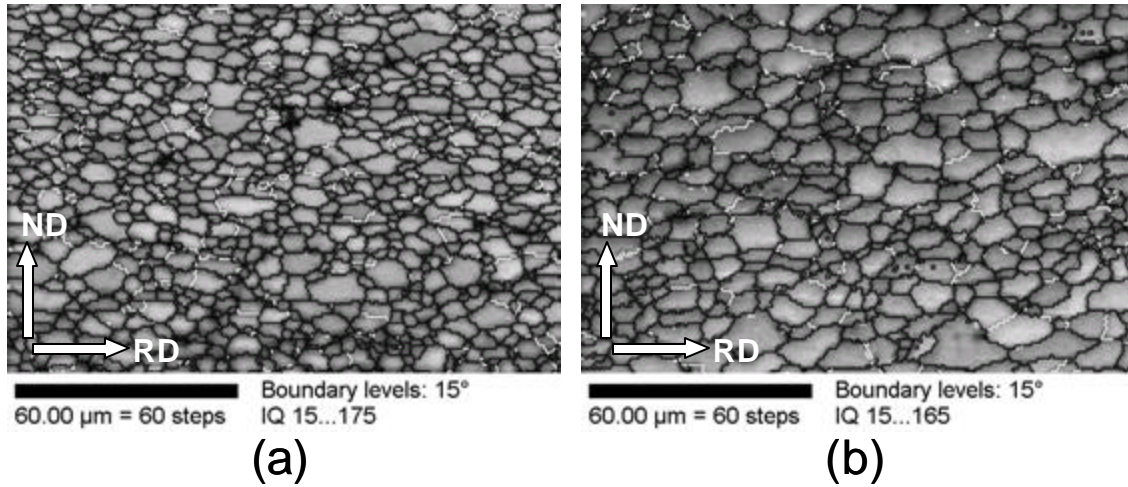
Figure 29.   Example grain maps showing (a) C4-1 and (b) D4-4

Table 5.   Table of results including statistical calculated values

Sample	Cold Roll Strain	Annealing Time (hr)	Grain Size (microns)	Standard Error	Standard Deviation
C4-1	2.37	100	5.66	0.03	1.47
C4-3	2.36	25	5.06	0.03	1.77
C4-4	2.35	1	5.78	0.03	1.81
D4-1	1.73	100	7.19	0.05	2.05
D4-2	1.76	25	6.55	0.05	1.59
D4-3	1.76	1	7.74	0.04	2.26
D4-4	1.41	100	7.76	0.05	2.16
D4-5	1.41	25	7.07	0.03	1.88
D4-6	1.40	1	6.63	0.03	1.81

C.   EFFECT OF COLD ROLLING

Figure 30 is a plot of each the grain size of each sample compared as a function of cold-rolling strain.
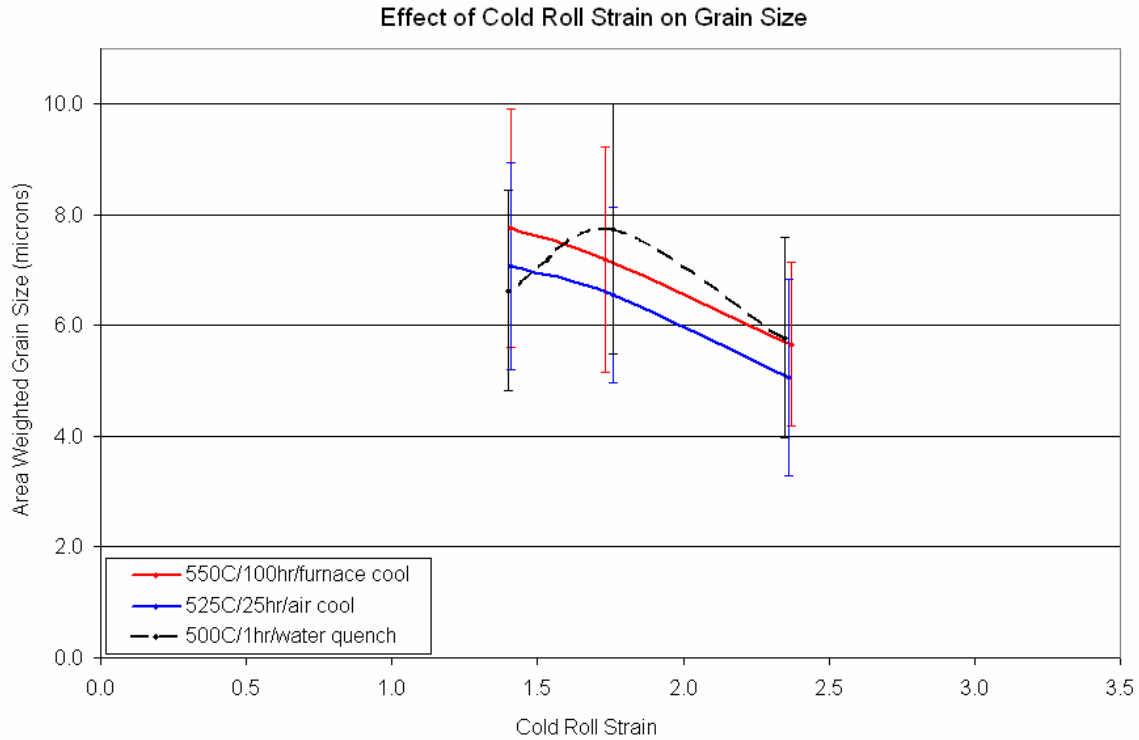
Figure 30.   Results from the recrystallization study of the effect of cold-rolling strain

The general trend in the data as seen by the central tendency lines for each annealing treatment shows that grain size is reduced as strain is increased. Because the grain size is a distributed and not a uniform quantity, this means that the peak of the distribution shifts towards the left (toward smaller grain sizes).

There is one point that does not agree with this trend (cold-rolling strain of 1.40 following annealing at 500°C). According to the PSN model, this point would not have a smaller grain size than the next higher strain (1.76) for the same annealing treatment. This suggests an alternate recrystallization mechanism.

In addition, this representation of the data makes it difficult to see the effect of annealing on the grain size.   At each strain value, it appears that the points, including the standard deviation, may differ by relatively small amount. This is investigated further using a different representation of the data.

37

D.   EFFECT OF ANNEALING SEVERITY

The same nine data points and corresponding standard deviations are plotted in Figure 31. The annealing is characterized by both time at temperature and cooling rate. Annealing severity increases as both annealing time increases and cooling rate decreases. Though many studies have been performed to investigate the effects of cold rolling, there is no general agreement on the effect of prior annealing on grain size. The data collected in this research shows that grain size has a weak dependence on the prior annealing treatment.

Particle stimulated nucleation theory predicts that there should be some optimum annealing treatment that would produce a large amount of nucleation sites without having the particles spread too far apart. This data weakly suggests this trend, where the intermediate heat treatment seems to give a minimum grain size for the higher two strains. The lowest strained data may have already reached its minimum grain size with its optimum treatment being even less severe. Otherwise, there is some other mechanism involved here.

Because the values of the means are so close together and the standard deviations are similar, the influence of prior annealing is minimal. It should be noted that cooling rates were also varied; the data for material annealed for 25 hours at 525°C followed by air cooling may give slightly finer grain sizes. The influence of cooling rate should be examined further.
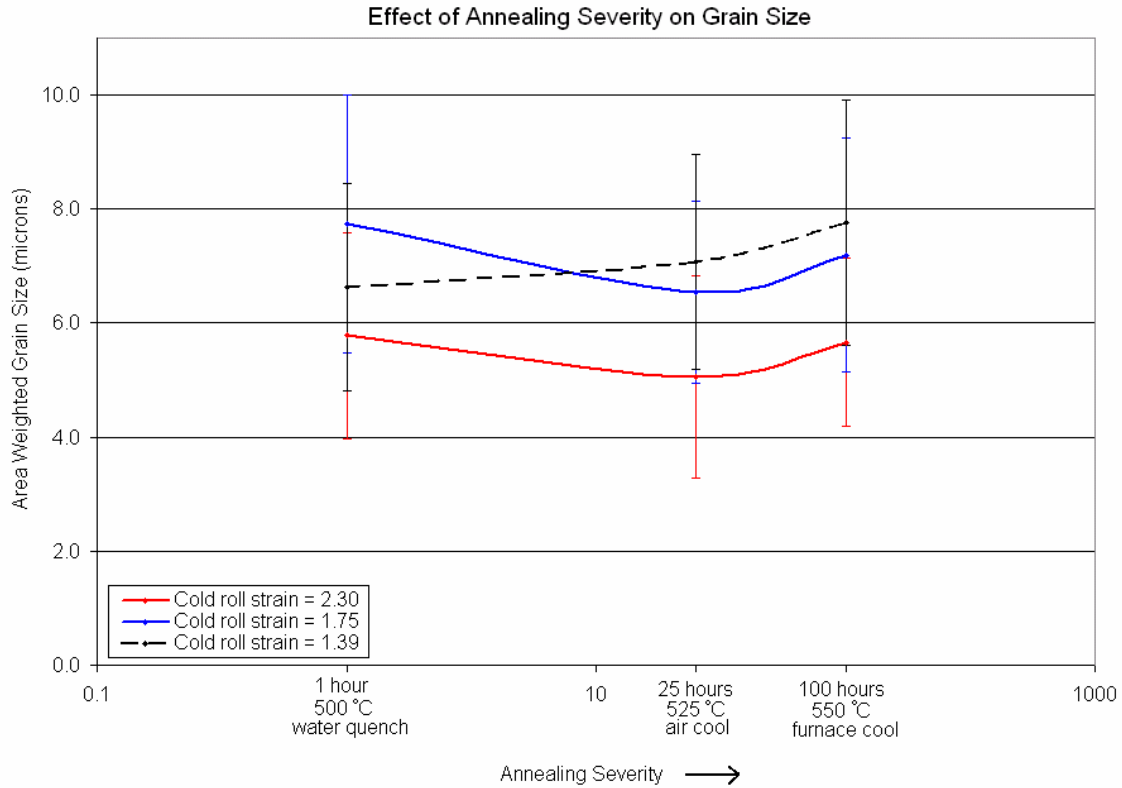
Figure 31.   Results from the recrystallization study of the effect of annealing

E.   ADDITIONAL OBSERVATIONS

The grain boundary sliding regime is typically characterized by a randomization of texture and a predominance of high-angle boundaries. The goal of the recrystallization treatment was to produce an initial microstructure having those characteristics. Although a completely random texture is desired, weak recrystallization textures are expected, as typical of rolled aluminum alloys.

Figure 32 shows a pole figure and an image quality map from one of the samples. The pole figure plots show a very weak texture as a concentration of points near the center of the {002} pole figure. In the software, these points were highlighted in red. All orientations within 5° of this orientation are highlighted with the corresponding grains simultaneously highlighted in the image quality map.

The recrystallization texture which developed in all nine samples was similar (as determined by intensity plots). The textured grains appeared in many cases to be randomly distributed although there are also contiguous groups in some areas and these groups tend to be aligned with the rolling direction.

Overlaid on the image quality plot are black lines representing high-angle boundaries and white lines representing low-angle boundaries. In every sample, over 87% of the boundaries were high-angle in nature. The remaining low-angle boundaries tend to occur in cube-oriented grains; this may reflect incomplete recrystallization by particle stimulated nucleation and a contribution from mechanisms involved in cube-grain formation.
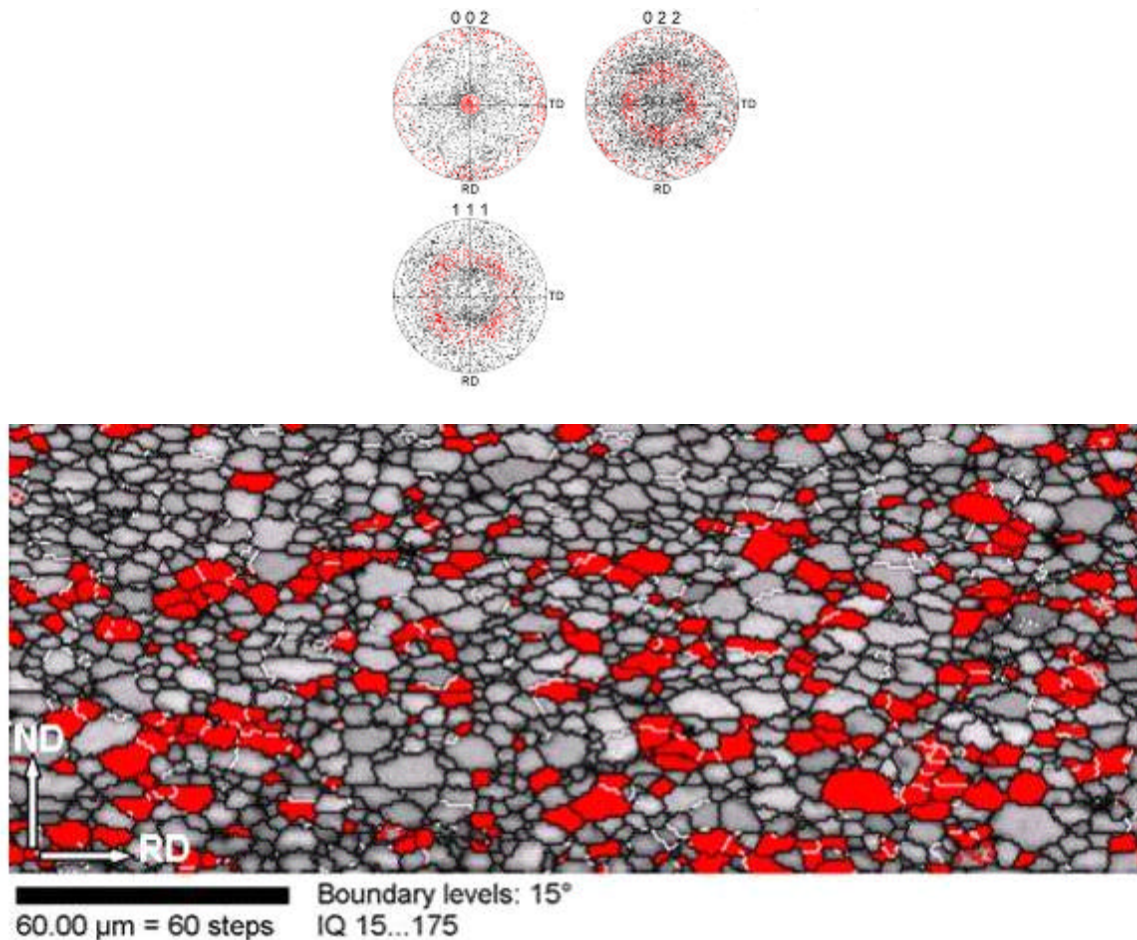

Figure 32.   Pole figure and image quality map for a sample; areas of high concentration on pole figure are highlighted; corresponding grains are highlighted in map (misorientation lines overlaid; =15° black, <15° white, 250 µm by 100 µm area, C4-1)

F. LIMITATIONS OF THE RECRYSTALLIZATION STUDY

1. Modeling of Engineering Alloy with Theory Developed for Dilute Alloys

AA5083 is an engineering alloy, thus containing impurities from casting. The original PSN model created by Humphreys was for a binary, dilute alloy. Once other elements are introduced into the alloy, complications will arise in predicting behavior: other phases may result or complex intermetallic particles that can have a large effect on material behavior.

2. Modeling of Superplastic Forming with Static Recrystallization

Although it is desired that the recrystallization treatment be representative of a superplastic forming process, in reality it simulates only the thermal cycle of the treatment. The stress and strain states have a complex relationship with the grain size and shape that is still not fully understood yet. Once the recrystallization study has been completed, the further studies should look into high temperature testing of the cold rolled materials. This would provide a useful comparison for the recrystallization study, as well as further information on recrystallization under both temperature and stress.

3. Second Phase Particle Distribution

Figure 32 shows an image quality map from a scan performed on a hot rolled sample. The second phase particles can be seen as dark areas in the image. Without detailed knowledge of the size and distribution of these second phase particles, it is not possible to completely determine the extent that second phase particles played in the recrystallization. The next step in this research must be determination of the size and size distribution of these particles.
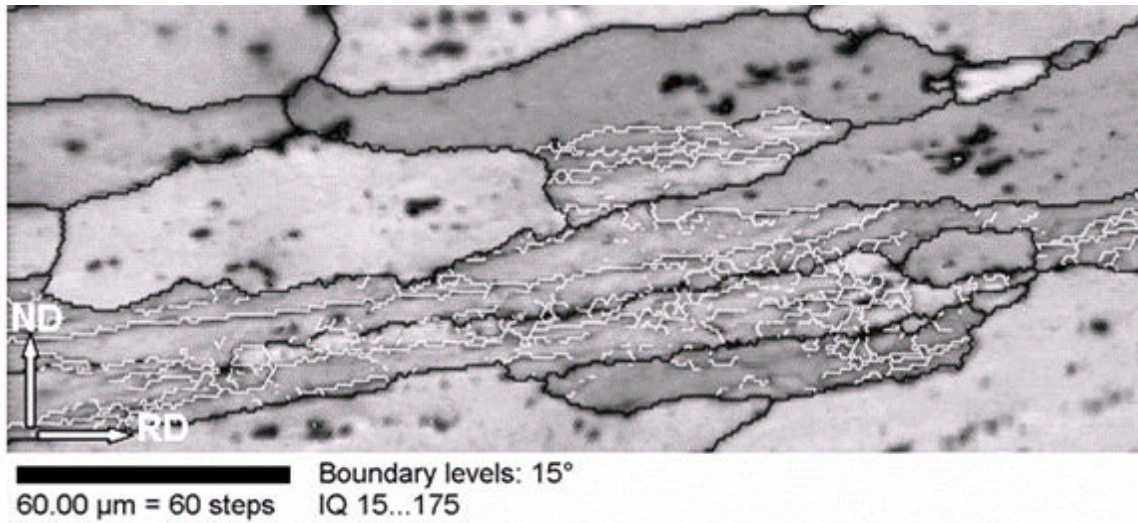
Figure 33.   Image quality map representing a hot rolled sample
(misorientation lines overlaid; =15° black, <15° white, 250 µm by 100 µm area, C4-1)

V. CONCLUSIONS

A. CONCLUSIONS

1. Effect of Cold Rolling

In general, an increase in cold-rolling strain decreased the grain size.

2. Effect of Annealing Treatment

The effect of the annealing treatment was difficult to determine given the standard deviation in the measurements. If the annealing did have an effect, it was minimal. Cooling rate is a potential factor in grain size as well.

3. Application of PSN Model

Though particle stimulated nucleation can explain some of the trends in the data, it is likely not the only mechanism affecting the recrystallization.

B. RECOMMENDATIONS FOR FUTURE WORK

1. Second Phase Particle Distribution

In order to determine how active the second phase particles were in the recrystallization, a thorough investigation into their size and distribution is necessary.

2. High Temperature Tests

Because superplasticity does not only subject a material to high temperature, but to tensile stresses as well, it would be useful to take samples from the processed material and perform high temperature testing to determine the superplastic response of the material. This would be especially useful in the extreme conditions to determine if the apparent change in grain size affects the superplastic response.

3. Statistical Analysis

Though previous work has modeled second phase particle distributions as lognormal in nature, it will be beneficial to determine if other distribution functions represent the data more accurately. Though a lognormal distribution models growth more accurately than a normal distribution, it may not have been the best fit possible as evidenced by the large error bars.

4.   Optical Microscopy

In addition to evaluating statistical methods employed, optical microscopy could be performed to validate the grain size measurements obtained through OIM. This data could further support the results obtained.

VI. LIST OF REFERENCES

[1]   Nieh, T.G., Wadsworth, J., and Sherby, O.D. *Superplasticity in Metals and Ceramics*. 1st ed., Cambridge University Press, 1997.

[2]   Sherby, O.D. and Wadsworth, J. "Development and Characterization of Fine-Grain Superplastic Materials". *Deformation, Processing, and Structure*. p.355-387.

[3]   SuperformUSA, http://www.superform-aluminium.com/susa/, Accessed June 2004.

[4]   Oh-ishi, K., Boyden, J.F., and McNelley, T.R. *Advances in Superplasticity and Superplastic Forming*. The Minerals, Metals, & Materials Society, 2004.

[5]   Kulas, M.A. *Mechanical and Microstructural Characterization of AA5083 Aluminum Alloys*. Doctor of Philosophy Dissertation, University of Texas at Austin, Austin, TX, May 2004.

[6]   Rehrmann, J. "Superplastic Forming: A Broad Technology Base for Enabling the Formation of Aluminum, Titanium, and Steel into Complex Components". http://www.boeingtechnology.com/docs/SPF_final.pdf, Accessed June 2004.

[7]   McNelley, T.R., Swisher, D.L. and Pérez-Prado, M.T. *Metallurgical and Material Transactions A*. v.33A, p. 279-290, 2002.

[8]   McNelley, T.R. *Deformation, Processing, and Properties of Structural Materials*. The Minerals, Metals, & Materials Society, 2000.

[9]   Pérez-Prado, M.T., González-Doncel, G., Ruano, O.A., McNelley, T.R. *Acta Materialia*. v.49, p.2259-2268, 2001.

[10]   Wert, J.A., Paton, N.E., Hamilton, C.H., and Mahoney, M.W. *Metallurgical Transactions A*. v.12A, p.1267-1276, 1981.

[11]   "AluSelect Composition Details". AluMatter website, http://aluminium.matter.org.uk/aluselect/06_composition_browse.asp, Accessed May 2004.

[12]   Montgomery Jr., J.P. *Advances in Superplasticity and Superplastic Forming*. The Minerals, Metals, & Materials Society, 2004.

[13]   Taleff, E.M. and McNelley, T.R. Private communication, May 2004.

[14]   *Metals Handbook: Metallography and Microstructures*. vol. 9, 9th ed., American Society for Metals, Materials Park, OH, 1987.

[15]   Christian, J.W. *The Theory of Transformations in Metals and Alloys.* 1st ed., Pergamon Press, 1965.

[16]   Doherty, R.D., Hughes, D.A., Humphreys, F.J., Jonas, J.J, Juul Jensen, D., Kassner, M.E., King, W.E., McNelley, T.R., McQueen, H.J., and Rollett, A.D. *Materials Science and Engineering A*. vol. A238, p. 217-274, 1997.

[17]   Kuhlmann-Wilsdorf, D. and Hansen, N. *Scripta Metallurgica et Materialia*. v.25, p.1557-1562, 1991.

[18]   Gorelik, S.S. *Recrystallization in Metals and Alloys*. Translation from Russian 1st ed., 1978, by Afanasyev, V., 2nd ed., Mir Publishers, 1981.

[19]   Cotterill, P. and Mould, P.R., *Recrystallization and Grain Growth in Metals*. 1st ed., Surrey University Press, 1976.

[20]   Hughes, D.A. Proceedings from "ReX 96: The Third International Conference on Recrystallization and Related Phenomena". Naval Postgraduate School, Monterey, CA, p.171-178, 1996.

[21]   Zhu, Q, and Sellars, C.M, Proceedings from "ReX 96: The Third International Conference on Recrystallization and Related Phenomena". Naval Postgraduate School, Monterey, CA, p.195-202, 1996.

[22]   McNelley, T.R., McMahon, M.E., and Hales, S.J. *Scripta Materialia*. v.36, no.4, p.369-375, 1997.

[23]   Humphreys, F.J. *Acta Materialia*. v.45, no.12, p.5031-5039, 1997.

[24]   Humphreys, F.J. *Acta Metallurgica et Materialia*. v.25, p.1323, 1977.

[25]   Stancey, S.L. "Assesment of Grain Refinement by Microstructure Analysis in Thermomechanically Processes AL 2519 Alloy". Master's Thesis, Naval Postgraduate School, Monterey, CA, 1987.

[26]   Reynolds Metal Company, *Heat Treating Aluminum Alloys*. Louisville, KY, 1954.

[27]   *Metals Handbook: Metallography, Structures, and Phase Diagrams.* vol. 8, 8th ed., American Society for Metals, Materials Park, OH, 1976.

[28]   Harrell, J.W. "Analysis of the Transition in Deformation Mechanisms in Superplastic 5083 Aluminum Alloys by Orientation Imaging Microscopy". Master's Thesis, Naval Postgraduate School, Monterey, CA, 2001.

[29]   *OIM Data Collection User's Manual.* TexSEM Laboratories, Draper, UT, 2001.

[30]   Randle, V. and Engler, O. *Introduction to Texture Analysis: Macrotexture, Microtexture, & Oreintation Mapping.* Gordon and Breach Science Publishers, 2000.

[31]   *OIM Analysis User's Manual.* TexSEM Laboratories, Draper, UT, 2001.

[32]   Aitchison, J. and Brown, J.A.C., *The Lognormal Distribtuion (with special reference to its uses in economics).* 1st ed., Cambridge University Press, 1957.

[33]   Lofton, B.J. "An Introduction to Stochastic Modeling". Summit Strategies Group, St. Lous, Mo, Jan. 2004.

[34]   "Exploratory Data Analysis". *NIST/SEMATECH e-Handbook of Statistical Methods.* National Institute of Standards and Technology, http://www.itl.nist.gov/div898/handbook/, Accessed May 2004.

THIS PAGE INTENTIONALLY LEFT BLANK

VII. INITIAL DISTRIBUTION LIST

1.   Defense Technical Information Center
        Ft. Belvoir, Virginia

2.   Dudley Knox Library
        Naval Postgraduate School
        Monterey, California

3.   Engineering and Technology Curricular Office, Code 34
        Naval Postgraduate School
        Monterey, California

4.   Department Chairman, Code ME/Hy
        Naval Postgraduate School
        Monterey, California

5.   Professor Terry R. McNelley, Code ME/Mc
        Naval Postgraduate School
        Monterey, California

6.   Dr. Keiichiro Oishi, Code ME/Oi
        Naval Postgraduate School
        Monterey, California

7.   Dr. Alex Zhilyaev, Code ME
        Naval Postgraduate School
        Monterey, California

8.   Professor Eric Taleff
        The University of Texas at Austin
        Austin, Texas

9.   Dr. Paul E. Krajewski
        General Motors Corporation
        Warren, Michigan

10.   Assistant Professor Michelle A. Koul
        Mechanical Engineering Department
        Annapolis, Maryland

11.   ENS Kristen L. Deffenbaugh
        Naval Postgraduate School
        Monterey, California